

Detailed budget analysis of HONO in central London reveals a missing daytime source

J. D. Lee^{1,2}, L. K. Whalley^{3,4}, D. E. Heard^{3,4}, D. Stone⁴, R. E. Dunmore², J. F. Hamilton², D. E. Young^{5,*}, J. D. Allan^{5,6}, S. Laufs⁷ and J. Kleffmann⁷.

[1] National Centre for Atmospheric Science, WACL Building, University of York, York, UK.

[2] Department of Chemistry, University of York, York, UK.

[3] National Centre for Atmospheric Science, University of Leeds, Leeds, UK.

[4] School of Chemistry, University of Leeds, Leeds, UK.

[5] School of Earth, Atmospheric and Environmental Sciences, University of Manchester, Oxford Road, Manchester, M13 9PL, UK.

[6] National Centre for Atmospheric Science, University of Manchester, Oxford Road, Manchester, M13 9PL, UK.

[7] Physikalische und Theoretische Chemie / Fakultät Mathematik und Naturwissenschaften, Bergische Universität Wuppertal (BUW), Gaußstr. 20, 42119 Wuppertal, Germany.

*now at: Department of Environmental Toxicology, University of California, Davis, CA 95616, USA.

Correspondence to: J. D. Lee (james.lee@york.ac.uk)

Abstract

Measurements of HONO were carried out at an urban background site near central London as part of the *Clean air for London* (ClearfLo) project in summer 2012. Data was collected from 22nd July – 18th August 2014, with peak values of up to 1.8 ppbV at night and non-zero values of between 0.2 and 0.6 ppbV seen during the day. A wide range of other gas phase, aerosol, radiation and meteorological measurements were made concurrently at the same site, allowing a detailed analysis of the chemistry to be carried out. The peak HONO / NO_x ratio of 0.04 is seen at ~02:00 UTC, with the presence of a second, daytime peak in HONO / NO_x of similar magnitude to the night-time peak suggesting a significant secondary daytime HONO source.

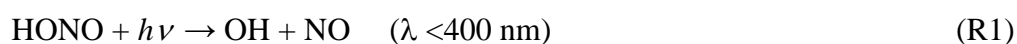
A photostationary state calculation of HONO involving formation from the reaction of OH and NO and loss from photolysis, reaction with OH and dry deposition shows a significant underestimation during the day, with calculated values being close to zero, compared to the measurement average of 0.4 ppbV at midday. The addition of further HONO sources from the literature, including dark conversion of NO₂ on surfaces, direct emission, photolysis of ortho-substituted nitro phenols, the postulated formation from the reaction of HO₂×H₂O with NO₂, photolysis of adsorbed HNO₃ on ground and aerosols, and HONO produced by photosensitized conversion of NO₂ on the surface increases the daytime modelled HONO to 0.1 ppbV, still leaving a significant missing daytime source. The missing HONO is plotted against a series of parameters including NO₂ and OH reactivity (used as a proxy for organic material), with little correlation seen. Much better correlation is observed with the product of these species with j(NO₂), in particular NO₂ and the product of NO₂ with OH reactivity. This suggests the missing HONO source is in some way related to NO₂ and also requires sunlight. Increasing the photosensitized surface conversion rate of NO₂ by a factor of 10 to a mean daytime first order loss of $\sim 6 \times 10^{-5} \text{ s}^{-1}$ (but which varies as a function of j(NO₂)) closes the daytime HONO budget at all times (apart from the late afternoon) suggesting that urban surfaces may enhance this photosensitized source. The effect of the missing HONO to OH radical production is also investigated and it is shown that the model needs to be constrained to measured HONO in order to accurately reproduce the OH radical measurements.

1 Introduction

The hydroxyl radical (OH) is the main daytime oxidant in the troposphere, playing a key role in the chemical transformations of trace species (Levy II, 1971). A major source of OH, especially in polluted environments, is the photolysis of nitrous acid (HONO) in the near UV region (R2). It has been shown in numerous studies that HONO can actually be the dominant early morning source of OH (Ren et al., 2003; Ren et al., 2006; Dusanter et al., 2009; Michoud et al., 2012) and has often been shown to also be significant during the rest of the day (Elshorbany et al., 2009; Hofzumahaus et al., 2009; Villena et al., 2011; Michoud et al., 2014). This is mainly due to unexpectedly high levels of HONO measured during daylight hours when fast photolysis would have been expected to keep concentrations low and hence insignificant for a source of OH. As a result of these studies, it has become clear that HONO

has the ability to initiate and accelerate daytime photochemistry and hence knowledge of its formation and loss are crucial to understanding tropospheric oxidation chemistry.

Typically, HONO in the troposphere would be expected to be governed by formation by the reaction between nitric oxide (NO) and OH (R2) and losses by photolysis (R1) and oxidation by OH (R3).



These reactions can be used, along with measurements of concentrations of the relevant species and HONO photolysis rates, to calculate a photochemical steady state concentration of HONO. Such calculations from field studies typically show a peak of HONO at night (when there is no photolysis), with levels in the low pptv range during the day. However, measurements usually show that daytime HONO levels can reach substantially higher concentrations than this, with mixing ratios up to a few hundred pptv frequently observed (Zhou et al., 2002; Kleffmann et al., 2005; Acker et al., 2006). It is clear from these analyses that there is an extra source of HONO present, which can have a significant impact on the atmospheric oxidising capacity due to its potential to form OH. A range of reactions have been postulated during the various studies to account for the missing source of HONO, with these likely to be heterogeneous either on aerosols or the ground itself. Major ground surfaces were recently confirmed by direct flux measurements of HONO (Ren et al., 2011; Zhou et al., 2011; Zhang et al., 2012). Tower measurements (Harrison and Kitto, 1994; Kleffmann et al., 2003; Oswald et al., 2015; Sörgel et al., 2011a, 2015; Stutz et al., 2002; Vandenboer et al., 2013; Villena et al., 2011; Vogel et al., 2003; Wong et al., 2012; Young et al., 2012), and aircraft observations (Li et al., 2014; Zhang et al., 2009) have also demonstrated that major HONO sources exist at canopy or ground surfaces through the measurement of vertical gradients. It is postulated that such processes involve the conversion of nitrogen dioxide (NO₂) or nitric acid (HNO₃) to HONO on ground surfaces and are enhanced by sunlight, thus providing a daytime only source of HONO (Zhou et al., 2003; George et al., 2005). In addition, bacterial production of nitrite in soil surfaces were also proposed as additional

HONO source (Su et al., 2011, Oswald et al., 2013). It has also been shown that HONO is emitted directly from petrol and diesel vehicle exhausts (Kurtenbach et al., 2001; Li et al., 2008). At most sites, this is a relatively small contributor to HONO due to its relatively short atmospheric lifetime in the daytime (10-20 minutes), however close to major roads and especially in tunnels it can contribute greatly to the HONO present. A recent publication by Michoud et al. (2014) gives a good summary of the possible daytime HONO sources under similar conditions to this study (in Paris) and a review by Kleffmann (2007) also discusses daytime HONO sources in depth.

Almost all previous field studies still show a significant missing daytime HONO source, thus showing the requirement for more studies. In this work we report what are, to our knowledge, the first measurements of HONO made in London, UK, one of the largest cities in Europe. The measurements were made as part of the summer intensive operation period of the *Clean Air for London* (ClearfLo) project and, as a result, were made concurrently with a wide range of other atmospheric gas and aerosol phase species (including OH, HO₂, NO, NO₂ and photolysis rates). This has enabled us to undertake a detailed modelling study of HONO using the Master Chemical Mechanism (MCMv3.2), in which we have included a series of known sources of HONO found in the literature. We then investigate the difference between daytime measured and modelled HONO, with a simple correlation analysis against other measured parameters. The model was also used to assess the radical forming potential of the missing HONO, which can ultimately lead to increased production of secondary pollutants such as ozone (O₃) and secondary organic aerosol (SOA).

2 Experimental

The ClearfLo project had the aim of providing an integrated measurement and modelling program in order to help better understand the atmospheric processes that affect air quality (Bohnenstengel et al., 2014). As part of ClearfLo, a summer intensive operation period (IOP) took place in July and August 2012, which involved the measurement of a wide range of gas and aerosol phase species (including meteorology), which enabled a detailed study of the atmospheric chemistry of London's air to be carried out.

2.1 Site description

The main site for the IOP was an urban background site at the Sion Manning School in North Kensington, London, ($51^{\circ} 31' 16''$ N, $0^{\circ} 12' 48''$ W), which is situated in a residential area approximately 7 km west of central London (defined here as Oxford Street). Measurements of NO, NO₂ and total reactive nitrogen (NO_y), sulphur dioxide (SO₂), O₃, carbon monoxide (CO), PM₁₀ and total particle number concentration have been routinely made at the site since January 1996 as part of the Automatic Urban and Rural Network (AURN) and the London Air Quality Network (LAQN) (Bigi and Harrison, 2010). For the ClearfLo IOP, other instruments were installed in various shipping container laboratories in the grounds of the school, all within 20 metres of the long term measurements. A full description of the campaign, including the instruments present can be found in (Bohnenstengel et al., 2014), however details of the measurements pertinent to this work are given below. All measurements were carried out at a height of around 5 metres above ground level, within a horizontal area of 10 metres from each other.

2.2 HONO measurements

HONO was measured using a long-path absorption photometer (LOPAP) instrument from the University of Wuppertal, Germany, which is explained in detail elsewhere (Heland et al., 2001). Briefly, gaseous HONO is sampled in a stripping coil containing a mixture of sulfanilamide in a 1M HCl solution and is derivatized into an azo dye. The light absorption by the azo dye is measured in a long path absorption tube by a spectrometer at 550 nm using an optical path length of 2.4 m. The stripping coil was placed directly in the atmosphere being sampled; meaning the length of the glass inlet was only 2 cm minimizing sampling artefacts. The LOPAP has two stripping coils connected in series to correct interferences. In the first coil (channel 1), HONO is trapped quantitatively together with a small amount of the interfering substances. Assuming that these interfering species are trapped in a similar amount in the second coil (channel 2), the difference between the signals of the two channels provides an interference-free HONO signal. Zero measurements were performed every 7 hours. Calibrations of the spectrometer using a known concentration of the derivatized azo dye were carried out 3 times during the campaign. The instrument was previously successfully validated against the spectroscopic DOAS technique under urban conditions and in a smog chamber (Kleffmann et al., 2006). During the campaign a detection limit of 1 pptV (for a time resolution of 5 min), a precision of 1 % and an accuracy of 10 % were obtained.

2.3 Radical measurements

OH, HO₂ and RO₂ radical concentrations were measured using the FAGE (fluorescence assay by gas expansion) technique (Heard and Pilling, 2003). In the case of HO₂ and RO₂, the radicals were first titrated with NO to OH before FAGE detection. The current mode of operation is described in detail elsewhere (Whalley et al., 2015a). The HO₂ observations used as a constraint in the modelling studies reported in section 3.3 were made using a low flow of NO (7.5 sccm), which laboratory tests have shown minimised interferences from alkene and aromatic-derived RO₂ species (Whalley et al., 2013). Under this regime, the interference from RO₂ radicals present is estimated to contribute <3 % to the HO₂ concentration. The limit of detection (LOD) at a signal to noise ratio of three for one data acquisition cycle was $\sim 1.3 \times 10^6$ molecule cm⁻³ for OH and $\sim 6.3 \times 10^6$ molecule cm⁻³ for HO₂. The measurements were recorded with 1 s time-resolution, and the accuracy of the measurements was ~ 15 %.

2.4 Other supporting measurements

The NO and NO₂ data used in this work were taken using an Air Quality Design Inc. custom built high sensitivity chemiluminescence analyser with LED based blue light NO₂ converter. The instrument consists of two channels measuring NO by reaction with excess O₃ to form excited state NO₂ followed by the detection of the resultant chemiluminescence (Drummond et al., 1985; Lee et al., 2009). The air flow in one of the channels first passes through a photolytic converter where light at 395 nm from an array of LEDs photolyses NO₂ to NO. The 395 nm wavelength has a specific affinity for NO₂ photolytic conversion to NO, giving high analyte selectivity within the channel and there is a low probability of other species (such as HONO) being photolysed (Pollack et al., 2010). This makes this measurement a significant improvement over the high temperature catalytic NO₂ conversion used for the long term measurement at the North Kensington site (Steinbacher et al., 2007; Villena et al., 2012). Calibration of the instrument was carried out every 2 days using 5 ppm NO in nitrogen (BOC – certified to NPL scale) - diluted to ~ 20 ppb using high purity zero air (BOC BTCA 178). The NO₂ conversion efficiency (ca. 40%) was calibrated using gas phase titration of the NO standard by O₃. NO_y data were taken using a TEI 42i TL NO analyser with Molybdenum converter.

VOC measurements were obtained using two gas chromatography (GC) instruments. The volatile fraction of VOCs (C_2 - C_7 hydrocarbons, with a small selection of OVOCs) was measured using a dual channel (DC)-GC-FID (flame ionization detector) (Hopkins et al., 2003), while a comprehensive two dimensional GC (GC \times GC-FID) measured the less volatile fraction (C_6 - C_{13} , with a large group of OVOCs) (Lidster et al., 2014).

Measurements of HCHO were made using an Aerolaser 4021 analyser (Salmon et al., 2008). Briefly, gaseous formaldehyde is scrubbed into the liquid phase via a stripping coil containing dilute sulphuric acid. This is followed by reaction with Hantzsch reagent, a dilute solution made with acetyl acetone, acetic acid, and ammonium acetate. Aqueous phase formaldehyde reacts with this reagent via the 'Hantzsch reaction' to produce 3,5-diacetyl-1,4-dihydrolutidine (DDL). Once excited by an appropriate wavelength (400 nm in this case), DLL fluoresces thus allowing quantitative assay by monitoring the emitted light.

Non-refractory PM_{1.0} nitrate, sulphate, organic matter, chloride and ammonium were quantified using a compact time-of-flight aerosol mass spectrometer (cToF-AMS - Aerodyne Inc.), which gave data with a time resolution of 5 minutes (Young et al., 2015). Ammonium is reflective of the overall ammonium nitrate because ammonium nitrate is both non-refractory and tends to be in the submicron fraction. While there is supermicron nitrate, it is overwhelmingly in the form of sodium nitrate, which is refractory and not measured by the AMS. It is specifically the nitrate measurement that is of interest here because it pertains to the working hypothesis.

Total aerosol surface area was calculated using data from an aerodynamic particle sizer (APS) instrument (TSI Inc, model 3321). The mean diameter of particles in each size bin (assume spherical) multiplied number of particles in that bin. In total there were 53 size bins ranging from 0.53 to 21.29 μ m. Actinic fluxes of solar radiation were measured using a spectral radiometer, which consisted of an Ocean Optics high resolution spectrometer (QE65000), couple via fibre optic to a 2π quartz collection dome. These measurements were then used to calculate the photolysis frequencies of a number of >50 trace gases, including NO₂, HONO and O₃ ($j(O^1D)$) (Kraus and Hofzumahaus, 1998; Edwards and Monks, 2003). Wind speed and direction, temperature and relative humidity were measured using a Davis Vantage Vue met station. Mixing heights estimation was based on the vertical profiles of the hourly vertical velocity variance (Barlow et al., 2011). The vertical velocity variance was measured with a Doppler Lidar (Halo-Photonics scanning Doppler lidar) located at the North Kensington site

with a gate resolution of 18 m; the un-sampled portion of the vertical velocity variance is calculated with the spectral correction technique described in (Barlow et al., 2015). The mixing height is defined as the height up to which the vertical velocity variance is higher than $0.1 \text{ m}^2 \text{ s}^{-2}$. This threshold value was perturbed by 20%, (i.e. between $0.08 \text{ m}^2 \text{ s}^{-2}$ and $0.121 \text{ m}^2 \text{ s}^{-2}$) and the median of the estimated values was taken as the hourly mixing height.

3 Results

3.1 Overview of data

Data were collected from 22nd July – 18th August 2012 and time series of local wind speed, wind direction, NO, NO₂, O₃, HONO and the photolysis rate of HONO ($j(\text{HONO})$) are shown in figure 1. The majority of the measurement period was characterised by south westerly winds, with the wind speed showing a diurnal cycle of less than 1 m s^{-1} at night (the minimum measurable by the anemometer) to $4 - 6 \text{ m s}^{-1}$ in late afternoon. These periods show NO and NO₂ with peaks of 15 ppbV and 10 ppbV respectively, typically at ~07:30 UTC, the peak of the morning rush hour. O₃ shows a diurnal cycle with a typical maximum of $40 - 45 \text{ ppbV}$ at ~16:00 UTC and minima of $<20 \text{ ppbV}$ at night. The exceptions to this are two periods from 24th – 27th July and 8th – 10th August, during which the site was subjected to generally easterly flow, with lower wind speed. Due to central London being to the East of the site, these periods are characterised by higher levels of NO_x (up to 60 ppbV of NO and 50 ppbV of NO₂), which has its source mainly from traffic exhaust. O₃ is also higher during these periods, due to a combination of the higher primary pollution levels (NO_x and VOCs) and low wind speeds causing a build-up of this secondary pollutant during the 3-4 day period. Peak daytime levels of O₃ of $60 - 100 \text{ ppbV}$ are observed during these more polluted periods. HONO concentrations show peak values at night throughout the campaign (up to 1.8 ppbV during the easterly periods and up to 0.7 ppbV during the rest of the campaign), with non-zero values seen during the day ($0.3 - 0.6 \text{ ppbV}$).

This behaviour is better visualised using the average diurnal cycle, which is shown for HONO and NO_x in figure 2(a) and $j(\text{HONO})$ and the HONO / NO_x ratio in figure 2(b). As well as the total campaign average, diurnal cycles are shown for the easterly and westerly time periods described above. NO_x follows an expected profile, with a peak of 29 ppbV on average during the morning rush hour at ~05:30 UTC (06:30 local time), followed by a decrease during the day, due largely to increasing boundary layer depth and hence dilution. After ~16:00 UTC,

1 the NO_x levels begin to rise from a minimum of 8.5 ppbV, due to a combination of increased
2 emissions during the evening rush hour and the reduction of the boundary layer depth into the
3 night. Concentrations reach ~ 18 ppbV by midnight and remain reasonably constant
4 throughout the rest of the night. Diurnal averages in the easterly and westerly conditions
5 follow the same pattern as for the total data series, with significantly higher NO_x during the
6 easterly period. During the morning peak, NO_x is a factor of 3 higher during easterly flow
7 compared to westerly and 15 - 20 % higher during the daytime. HONO appears to follow a
8 similar diurnal profile to NO_x , which is not unexpected since the main known HONO sources
9 involve nitrogen oxides. However, the morning peak of HONO is around 1 hour earlier
10 compared to NO_x (at around 04:30) due to the onset of HONO photolysis at sunrise. HONO
11 concentrations are also higher under easterly flow conditions compared to westerly, with the
12 early morning peak being a factor of around 2 higher and the daytime average around 25%
13 higher. The behaviour of HONO is perhaps better described by looking at the $\text{HONO} / \text{NO}_x$
14 ratio and the average diurnal cycle of $\text{HONO} / \text{NO}_x$ and $j(\text{HONO})$ is shown in figure 2b. The
15 peak $\text{HONO} / \text{NO}_x$ of 0.04 is seen at $\sim 02:00$ UTC, due to the lack of photolysis (the major
16 loss route for HONO), direct HONO emissions and heterogeneous HONO formation at the
17 surface during the night, into a relatively shallow boundary layer. After this (and before
18 sunrise), the ratio begins to decrease due to the onset of fresh NO_x emissions and continues to
19 decrease during the morning due to the increase of HONO photolysis. If the HONO sources
20 which are active during night-time are the only active sources also during daytime, the
21 HONO/NO_x ratio should show a deep minimum around noon. In contrast, in figure 2 a
22 maximum is observed, which is a hint to an additional daytime source. In addition, the
23 maximum of HONO/NO_x correlates well with the radiation, which is again a hint for a
24 photochemical process.

25 The HONO levels measured in London are within the range of data published from other
26 urban sites, although there is a wide range of concentrations reported in the literature.
27 Michoud et al., 2014 reported daytime levels of 0.11 ppbV (averaged for 3 hours around local
28 solar noon) at a site near Paris, France, which is lower than our value of 0.44 ppbV. However
29 the site was 14 km from the centre of Paris (upwind), significantly further away from the
30 major emission sources than the London site. As a result, NO_x was lower in Paris, with a
31 daytime campaign average of 5.3 ppbV compared to our value of 13.9 ppbV, giving a daytime
32 $\text{HONO} / \text{NO}_x$ ratio of 0.020 compared to our value of 0.031, although this may be partially
33 explained by the lower $j(\text{HONO})$ values in London compared to Paris. The fact that the

London site is closer to emission sources will most likely also influence this, as direct emission of HONO from traffic exhaust is potentially a significant proportion of HONO in large cities (Kurtenbach et al., 2001). Kleffmann et al., 2006, reported daytime HONO levels of between 0.2 – 0.3 ppbv in Milan, Italy. They also compared data from a LOPAP instrument (similar to that used in this study) and a Differential Optical Absorption Spectroscopy (DOAS) instrument and showed excellent agreement. The resultant HONO / NO_x ratio reported was 0.046. Wong et al., 2012, reported daytime HONO mixing ratios averting 0.1 ppbv in Houston, USA, with corresponding average daytime NO_x of 10 ppbv, giving a HONO / NO_x ratio of 0.03. Some other studies in large cities have reported larger daytime HONO concentrations, e.g. Santiago, Chile (1.5 ppbV) (Elshorbany et al., 2009), Guangzhou, China (2.0 ppbV) (Qin et al., 2009) and Xinken, China (0.80 ppbV) (Su et al., 2008a; Su et al., 2008b), however, all of these were at sites with much larger NO_x loading and so the resultant HONO / NO_x ratio is similar to the measurements in London. The range of ambient HONO values reported in the literature suggest that the specific conditions at a particular site are key to the HONO levels, in particular the prevalence of different levels of NO_x during daylight hours. Thus a modelling study including a range of known HONO sources and sinks is required to fully understand the observed behaviour.

3.2 HONO photostationary state approach

In order to initially assess HONO concentrations and in particular the impact of any potential extra sources during this campaign, a photostationary state (PSS) calculation has been carried out. In this approach, the sources and sinks of the species in question are assumed to balance each other and is thus only suitable for species with a short lifetime, such as free radicals. However, it has been widely used to study the daytime HONO budget, despite its lifetime being in the range of 10 – 20 minutes during the day (Alicke et al., 2002; Wong et al., 2012), resulting in significant uncertainties, especially for measurements close to emission sources (Lee et al., 2013). However, the measurement site in this study is described as an urban background site and thus is relatively free from the influence of major roads or point sources. Calculation of the transport time since emission using the NO_x / NO_y ratio (using the technique described in (Cappa et al., 2012)) shows a lifetime since emission of 40-50 minutes, significantly greater than the photochemical lifetime of HONO (typically 10 - 20 minutes at noon). Thus, we consider the PSS approach still as a useful tool to quantify HONO sources

during daytime. HONO is expected to be in photostationary state due to its formation by the reaction between OH and NO, and its sinks by rapid photolysis (to reform OH and NO), its reaction with OH and its dry deposition. Combining these terms, the concentration [HONO]_{PSS} can be calculated using the following equation (1):

$$\text{HONO}_{\text{PSS}} = \frac{k_{\text{OH}+\text{NO}}[\text{OH}][\text{NO}]}{k_{\text{OH}+\text{HONO}}[\text{OH}] + j(\text{HONO}) + \frac{v_{\text{HONO}}}{h}} \quad (1)$$

Measured data were used for OH, NO and $j(\text{HONO})$, with the relevant pressure and temperature dependant rate constants for $k_{\text{OH}+\text{NO}}$ and $k_{\text{OH}+\text{HONO}}$ taken from (Atkinson et al., 2004). v_{HONO} is the deposition velocity of HONO, set at an upper limit of 3.0 cm s^{-1} , and h is the boundary layer height. We use an effective HONO boundary layer height (BL) of 75 m, calculated using typical Eddy diffusion coefficients and $j(\text{HONO})$, as the likely height to which HONO will reach, given a daytime lifetime of 15 minutes. This method will strongly underestimate HONO deposition because the boundary layer height will be considerably larger than the height at which HONO will actually be transported to, due to its short lifetime (10-20 minutes during the day). This effect is partly compensated for by using 3.0 cm s^{-1} for the deposition velocity, which is at the upper end of the ranges quoted in the literature (Harrison and Kitto, 1994; Stutz et al., 2002; Trebs et al., 2006); however it does mean there are considerable errors in this approach. The PSS analysis also does not consider vertical structure, thus the magnitude of any unknown source inferred from the analysis will be dependent on the height above the ground surface that the measurements are being made. The average daytime diurnal profiles in both easterly and westerly conditions are shown in figure 3. We do not consider night time data as the PSS approach would not be valid at night. We only consider data from 08:00 UTC ($j(\text{HONO}) > 4 \times 10^{-4} \text{ s}^{-1}$), a time at which all HONO produced during the night will have been lost due to photolysis after sunrise. It is clear that the PSS calculation cannot replicate the measured HONO during daylight hours (08:00 – 20:00 UTC). The PSS does appear to reproduce the daylight cycle of HONO, with high concentrations during the morning peak between 06:00 and 09:00, due to the increase in NO and OH at the morning rush hour. However, after this morning peak, HONO_{PSS} rapidly decreases to $<0.05 \text{ ppbV}$ by midday, followed by a gradual decrease during the afternoon reaching a minimum of 0.007 ppbv at 19.30. This is due to the rapid photolysis of HONO,

which occurs in the near UV region, and occurs significantly faster than the only production route in the PSS calculation ($\text{OH} + \text{NO}$), especially during the later part of the day when NO is low. HONO_{PSS} during the day shows similar levels in both easterly and westerly conditions, despite measured HONO being significantly higher in the more polluted easterly regime. The PSS treatment of HONO is clearly incomplete, with significant missing source terms.

3.3 HONO box model approach

In order to assess the importance of other potential HONO sources in our study, we use a photochemical model based on the Master Chemical Mechanism (MCMv3.2) (Jenkin et al., 2012). Complete details of the kinetic and photochemical data used in the mechanism are available at the MCM website (<http://mcm.leeds.ac.uk/MCM/home>). The model was run with a sub-set of the MCM and treated the degradation of simultaneously measured trace VOCs, CH_4 and CO following oxidation by OH, O_3 and NO_3 and included ~15,000 reactions and ~3,800 species. The model was constrained to measurements of NO, NO_2 , O_3 , CO, CH_4 , 62 individual VOC species measured by GC-FID and also 2D-GC, PAN, HCHO, HNO_3 , HO_2 , water vapour, temperature and pressure. The model was constrained with the measured photolysis rates (including $j(\text{O}^1\text{D})$, $j(\text{NO}_2)$, $j(\text{HONO})$, $j(\text{HCHO})$, $j(\text{CH}_3\text{COCH}_3)$ and $j(\text{CH}_3\text{CHO})$). A constant H_2 concentration of 500 ppbV was assumed (Forster et al., 2012). The model inputs were updated every 15 minutes. For species measured more frequently, data was averaged to 15 minute intervals, whilst those measured at a lower time resolution were interpolated. The loss of all non-constrained, model generated, species by a wind speed dependent deposition (v) was calculated by summing the resistances $1/R_a$, $1/R_b$ and $1/R_c$, for which R_a describes turbulent convective transport, R_b the laminar diffusion near the surface and R_c the surface resistance. The inverse of the surface resistances ($1/R_c$) assumed are 3 cm s^{-1} for HNO_3 and 2 cm s^{-1} for HONO and 1 cm s^{-1} for NO_2 (and all other non-constrained model species). For the campaign average wind speed of 1.6 m s^{-1} , v_{HNO_3} , v_{HONO} and v_{NO_2} equal 0.52, 0.48 and 0.38 cm s^{-1} respectively. As with the steady state approach, we use an effective HONO boundary layer height (BL) of 75 m in the model. This assumption leads to a campaign average first order loss of HONO (at a mean wind speed of 1.6 m s^{-1}) of $v_{\text{HONO}}/\text{BL} = 6.4 \times 10^{-5} \text{ s}^{-1}$. The model was run for the entirety of the campaign in overlapping 7 day segments. To allow all the unmeasured, model generated intermediate species time to reach steady state concentrations, the model was initialised with inputs from the first measurement

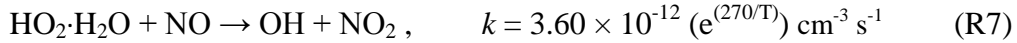
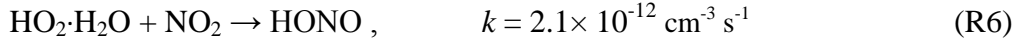
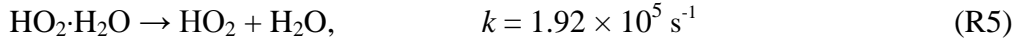
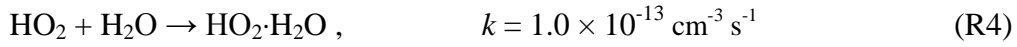
day (22nd July) for 5 days before comparison to measurements were made. Comparison of these 5 spin up days demonstrated that the concentration of model generated species rapidly converged and there was less than a 1% difference in (for example) modelled OH or HONO concentration by the second spin up day. As a result of this, the model segments were run so as to overlap for 2 days only to reduce the computing time. The model was run unconstrained to HONO (for the results presented in this paper) for comparison with measured HONO concentration.

A number of HONO sources in addition to the gas phase source from the reaction of hydroxyl radicals with NO have been included in the model. These include:

a.) A direct emission source of HONO was added to the model, using a ratio of HONO:NO_x of 0.008 reported previously from tailpipe emission studies of NO_x and HONO in a tunnel (Kurtenbach et al., 2001) and the measured NO_x concentrations. It is likely that the used value represents an upper limit of the direct emission contribution to HONO during daytime, due to the short atmospheric lifetime of HONO (10-20 minutes) compared to NO_x.

b.) It has been suggested that a reaction between HO₂×H₂O and NO₂ could produce HONO at a sufficiently fast rate to be a significant source in the troposphere (Li et al., 2014). It had previously been shown in laboratory studies that this reaction produces negligible HONO yields under dry conditions (Tyndall et al., 1995; Dransfield et al., 2001). However, in the lower troposphere, around 30% of HO₂ is suggested to be present as an HO₂·H₂O complex, and hence may show different chemical behaviour. Kinetic measurements of the self reaction HO₂ + HO₂ have revealed the chaperone effect of water vapour enhancing the rate coefficient (Stone et al., 2005). It has also been shown that the rate coefficient of the reaction HO₂+NO₂ increase by 50% from dry to humid atmospheric conditions (Sander and Peterson, 1984). In the Li et al. study it was postulated that the reaction converts NO₂ to HONO with a yield of 100% and this allowed a model to reproduce the observed levels of HONO, albeit under free tropospheric conditions away from surfaces. Inclusion of this reaction also improved the agreement between the model and measured levels of HO₂ and NO_x. However, recent field data has shown that in fact, this reaction produces only a 3% yield of HONO (Ye et al., 2015), thus greatly reducing the impact of the reaction on HONO production. Nevertheless, the following additional reactions were included in our MCM model to account for the equilibrium that exists between uncomplexed and H₂O-

complexed HO₂ in the atmosphere (R4 & R5) and the major reactions of H₂O-complexed HO₂ in this urban environment (R6 and R7):



c.) Light induced heterogeneous conversion of NO₂ to HONO on aerosol surfaces was also considered assuming an uptake coefficient of 10⁻⁶ (Kleffmann et al., 1999; Arens et al., 2001; Monge et al., 2010).

d.) Heterogeneous conversion of NO₂ to HONO on ground surfaces at a rate equal to ~2×10⁻⁸ s⁻¹ has been included in the model which is consistent with laboratory studies, which put an upper limit on dark surface source of <10⁻⁷, e.g. Stemmler et al. (2007). This was parameterised in the model by taking the wind-speed dependent ν_{NO_2} and assuming instantaneous mixing of surface emitted HONO up to a height of 75 m. This leads to a first order loss of NO₂ to the ground at a rate of 4 x 10⁻⁵ s⁻¹ on average. This rate was scaled down by a factor of 2000 to represent the dark surface conversion of NO₂ to HONO reported in laboratory studies. However, it has to be stressed, that the present calculation strongly underestimates the contribution of heterogeneous HONO formation on ground surfaces, especially during night-time at the measurement height, caused by the assumption of an instantaneous mixing up to a height of 75 m, see Eq 1.

e.) A daytime source from the photolysis of ortho nitro phenols which were not measured during the campaign but have been estimated to be present at an upper limit constant concentration of 1 ppbV and which photolyse at a rate of ~3 × 10⁻⁵ s⁻¹ at midday (Bejan et al., 2006).

f.) Photolysis of adsorbed HNO₃ on ground surfaces has been reported to produce HONO (Zhou et al., 2003; Zhou et al. 2011). We have estimated the concentration of HNO₃ deposited to the ground surface from the gas-phase HNO₃ concentration that was measured during ClearfLo and from the wind speed dependent ν_{HNO_3} (Zhou et al., 2011). To assess

the maximum impact of this potential HONO source, a noon photolysis rate of surface HNO_3 of $6 \times 10^{-5} \text{ s}^{-1}$, two orders of magnitude faster than $j(\text{HNO}_3)_g$ ($j(\text{HNO}_3)_{0^\circ\text{SZA}} = 6 \times 10^{-7} \text{ s}^{-1}$) in the gas phase, has been taken (Zhou et al., 2011) and a 100 % HONO yield was assumed.

g.) Photolysis of nitrate aerosols. To assess the maximum impact of this potential HONO source, a noon photolysis rate of aerosol NO_3^- of $6 \times 10^{-5} \text{ s}^{-1}$ and a 100 % HONO yield was again assumed.

h.) Photosensitised heterogeneous conversion of NO_2 to HONO on ground surfaces has been parameterised and included in the model by taking a ground surface conversion, which correlates with NO_2 photolysis. A wind speed dependent NO_2 deposition velocity calculated using $1/R_c = 1 \text{ cm s}^{-1}$ (Joyce et al., 2014) in 75 m BL leads to a first order loss of NO_2 to the ground at a rate of $4 \times 10^{-5} \text{ s}^{-1}$ on average, this is multiplied by a scaling factor equal to $0.25 \times j(\text{NO}_2)$ which leads to an overall photosensitized conversion of $\text{NO}_2 \rightarrow \text{HONO}$ of $\sim 5.6 \times 10^{-6} \text{ s}^{-1}$ during the day on average; consistent with the light induced conversion of NO_2 to HONO observed in laboratory studies on humic acid surfaces (Stemmler et al 2007).

We do not include desorption of adsorbed HONO from soil (Oswald et al., 2013, 2015; VandenBoer et al., 2013) as they are still largely speculative, depend on many uncertain variables (soil pH, bacterial activity, soil humidity) and most probably have a very minor contribution under our highly urban conditions (low soil coverage, different expected diurnal contribution).

The full time series of the modelled HONO using the MCM, along with the measured values for the entire measurement campaign are shown in figure 4. Due to the difficulties of predicting nighttime chemistry with a photochemical model (such as the MCM), we only consider here the daytime (08:00 – 20:00). The time series show that predicted daytime HONO using the full model is higher than from the simple PSS calculation, however, it can be seen that the predicted daytime HONO is still lower than the measurement on all days and falls outside the 10% error of the LOPAP instrument. The average daytime diurnal cycle of the measured and modelled HONO, along with the contribution of the different sources in the

model is shown in figure 5. From just after sunrise (08:00), the contribution to HONO of the reaction between OH and NO decreases quickly due to the increasing $j(\text{HONO})$ and decreasing NO levels throughout the morning. The largest contribution throughout the day comes from the photolysis of adsorbed HNO_3 , contributing around 50% of the HONO source at midday. There are small contributions during the day and from heterogeneous conversion of NO_2 (on both aerosol and ground surfaces) and the photolysis of ortho-nitro-phenol. Examining the total HONO predicted by the model compared to the measurement shows a significant underestimation of the modelled HONO compared to the measurement. They do both follow a similar diurnal cycle, with a decrease in HONO until around 16:00, followed by an increase into the evening, however the modelled HONO is up to a factor of around 2 lower than the measurement throughout the day. Subtracting the modelled from the measured HONO gives us a quantity that can be described as ‘missing’ HONO source, and average diurnal daytime profile of this is plotted in figure 6. The amount of the missing HONO source begins to increase at 08:00 and reaches a maximum at 12:00 of $\sim 2.8 \text{ ppbV hr}^{-1}$, exhibiting a similar diurnal trend to that of the HONO / NO_x ratio (see figure 2). It then starts to decrease throughout the afternoon and into the evening. Further analysis can be carried out by examining the diurnal profiles in the easterly and westerly flow conditions described earlier. Both conditions show broadly the same diurnal profile, however the daytime peak in missing HONO is greater in the more polluted easterly flow (up to 0.6 ppbV). This suggests that any missing source of HONO is related in some way to the pollution loading, most likely the amount of NO_2 . This will be discussed further in later sections.

It is clear from this data, that neither a photostationary state calculation nor a more complete photochemical model containing currently known and postulated sources of HONO (that are relevant for this environment) can reproduce the daytime levels measured in London during this study. This is potentially significant, as HONO can be a large source of free radicals in such an urban environment, and any missing source in models can lead to an underestimation of the oxidising capacity of the atmosphere, and hence its ability to produce O_3 . Therefore it is worth considering where the ‘missing’ HONO may come from and the importance of any extra source to the atmospheric oxidation capacity.

4 Discussion

4.1 Instrument interference

1 It is first worth considering the effect of possible instrument interferences on the HONO
2 measurements made in this study. As described earlier, the LOPAP technique is not direct
3 rather it measures HONO by conversion to a coloured azo dye which is then detected by
4 absorption spectroscopy. However, it has been postulated that HO_2NO_2 could interfere with
5 the conversion reaction, leading to erroneous HONO measurements. A recent study by
6 (Legrand et al., 2014), using an identical instrument to the one described here and
7 investigating apparently high measurements of HONO in Antarctica, showed in laboratory
8 experiments that the instrument does have an interference with HO_2NO_2 . Their work
9 indicated that up to 15% of HO_2NO_2 was converted to the azo dye in the instrument and
10 detected as HONO. For this study, 2 ppbv of HO_2NO_2 would explain the difference between
11 measured and modelled HONO, however this seems unrealistic in an urban environment in
12 summer (Dentener et al., 2002). In fact, the box model used here shows HO_2NO_2 levels to
13 only be between 2 – 10 pptv, therefore we feel that this instrument interference can be
14 discounted here. For submicrometer particles we exclude any interferences by particle nitrite,
15 since their sampling efficiency is $<2\%$ in the very short stripping coil (4 coil sampler). Even
16 if that increased to values of 10 % for larger coarse particles, such interference would be
17 almost perfectly corrected for by the two channel approach. For much larger fog particles
18 (which actually were not present during the campaign during daytime) interferences would be
19 only expected in the case of high fog pH values of >5 . For lower pH, expected for the urban
20 conditions in London, the effective solubility of HONO (HONO + nitrite) would be too low to
21 significantly influence the HONO data, even for high uptake efficiency of fog particles.
22 Accordingly, we do not consider particle interferences as an important issue. Finally, the
23 LOPAP was successfully inter-compared to the spectroscopic DOAS technique under urban
24 background conditions similar to the present study (Kleffmann et al., 2006).

26 **4.2 Missing HONO source**

27 The ClearfLo IOP campaign involved a wide range of measurements, thus enabling the
28 relationship between the apparent missing HONO and various other species to be
29 investigated. Initially, daytime diurnal average profiles were plotted for NO_2 and the product
30 $\text{NO}_2 \times j(\text{NO}_2)$, along with the extra rate of production of HONO required for the model to
31 reproduce the measurements (termed ‘missing HONO source’ - figure 7). The plots show that,
32 whilst there is little correlation between the NO_2 on its own with the missing HONO, there

appears to be a reasonable correlation with the product of NO_2 and $j(\text{NO}_2)$, hence pointing towards a photolytic source.

To further investigate any potential correlation, the full data series of the missing HONO source and different input data are normalised to 1 and correlated against each other. The normalised missing HONO source data are then correlated with the normalised products of all possible combinations of the input data. The datasets are then filtered to determine if inclusion of an extra dataset has led to a genuine increase in the correlation coefficient. For inclusion in the filtered output, the correlation coefficient for the product must be greater than the correlation coefficient for each of the individual components in the product. Additionally, inclusion of an additional dataset in a product must lead to an increase in the correlation coefficient for the new product when compared to the correlation coefficient without that new dataset. Datasets included are: $j(\text{NO}_2)$ (used as a proxy for radiation), water vapour, NO , NO_2 , temperature, adsorbed HNO_3 ($\text{HNO}_3_{\text{ads.}}$), OH , HO_2 , RO_2 , OH reactivity ($k(\text{OH})$), nitrate aerosol ($\text{NO}_3^-_{\text{aero.}}$), ammonium aerosol ($\text{NH}_4^+_{\text{aero.}}$) and aerosol surface area (SA). We use $k(\text{OH})$ as a proxy for organic substances as it has been shown by Whalley et al., 2015b, that $k(\text{OH})$ is largely controlled by VOCs during the measurement period (typically 80% during daytime). The correlation plots are shown in the supplementary information (figure S1), with the correlation coefficients of the different combinations presented in table 1. The data shows that several product combinations are significantly higher than those of the individual components. For instance, the correlation coefficient with NO_2 alone is virtually zero, whereas for the product of $j(\text{NO}_2) \times \text{NO}_2$ the r^2 is 0.696, for $j(\text{NO}_2) \times k(\text{OH})$ it is 0.678 and for $\text{NO}_2 \times k(\text{OH}) \times j(\text{NO}_2)$ the r^2 is 0.659. Thus, if gaseous VOCs (represented here by $k(\text{OH})$) are precursors for VOCs adsorbed onto surfaces, then this is an indication that the photosensitised reaction of NO_2 on surfaces containing organics as a source of HONO may currently be under-estimated in the model. We also see high correlation coefficients with $j(\text{NO}_2) \times T$ (0.628), however this can be explained by radiation and temperature following a similar diurnal pattern, albeit with a slight (1 - 2 hours) time lag. The product of $j(\text{NO}_2)$ and ammonium aerosol (NH_4^+) is 0.583, suggesting this may play a role in the missing HONO, although any possible mechanisms for this are unclear.

In order to investigate the day-to-day variation in the potential HONO source, correlation plots were made of the daytime average (08:00 – 20:00) missing HONO source against NO_2 and the product of $j(\text{NO}_2)$ with NO_2 , $k(\text{OH})$ and $\text{NO}_2 \times k(\text{OH})$ (figure 8). These show that

1 there is some correlation for all species, with the products of the species with $j(\text{NO}_2)$ ($r^2 =$
2 0.64, 0.55 and 0.71 for NO_2 , $k(\text{OH})$ and $\text{NO}_2 \times k(\text{OH})$ respectively) being significantly higher
3 than with NO_2 alone (r^2 0.33).

4 Based on the correlational analysis we propose here an enhancement in the photosensitized
5 conversion of NO_2 on organic substrates to explain the missing HONO source. In contrast,
6 other recently proposed HONO sources will have a minor contribution. Aqueous solutions in
7 which HONO yields from nitrate photolysis may be enhanced by organics (Scharko et al.,
8 2014) will be not important for the urban conditions investigated in this study as there are no
9 aqueous surfaces in the surrounding area. Or recently, in the study of Rutter et al. (2014), a
10 gas phase reduction of HNO_3 by VOCs to HONO was proposed. However, since the
11 conditions of that laboratory study were not atmospherically relevant (reaction in the presence
12 of ca. 200 ppb of a high molecular weight motor oil), we have not considered this source for
13 this analysis. In addition, this is a dark reaction, while we have mainly considered the more
14 important daytime HONO chemistry in the present manuscript. In the study of Ziemba et al.
15 (2010) a conversion of HNO_3 on organic aerosols was proposed based on field observations.
16 However, HONO formation was only observed in the dark, which again is out of the scope of
17 this study. In addition the very low correlation coefficient of the missing HONO source with
18 aerosol nitrate does not support this mechanism. Formation of HONO by soil sources (Oswald
19 et al., 2013, 2015) are also expected to be of minor importance for London, due to low soil
20 surface coverage.

21 Although direct emissions were already considered in the model, we carried out a sensitivity
22 analysis into the direct emission of HONO, to study potential errors within our model. We
23 found that increasing direct emissions by a factor of 2 (even though we think our estimate is
24 already an upper limit), only results in a 4% increase in the modelled HONO. Hence we do
25 not believe direct emissions to be the source of the missing HONO. We have also run a
26 sensitivity analysis on the heterogeneous photosensitized conversion of NO_2 on ground
27 surfaces by increasing the conversion rate by up to a factor of 10 to assess the impact of
28 enhanced reactive uptake of NO_2 on other surfaces, for example urban grime. We find that a
29 reactive conversion rate of $\sim 6 \times 10^{-5} \text{ s}^{-1}$ (but which varies as a function of $j(\text{NO}_2)$) closes the
30 daytime HONO budget at all times (apart from the late afternoon). This is shown in figure 9,
31 demonstrating that with an increased conversion rate, the heterogeneous photosensitized
32 conversion of NO_2 on ground surfaces becomes the largest HONO source throughout the day.

1 Based on this sensitivity study and on the high correlation of the missing HONO source with
2 the product $j(\text{NO}_2) \times \text{NO}_2$ and $j(\text{NO}_2) \times \text{NO}_2 \times k(\text{OH})$ enhanced photosensitized conversion of
3 NO_2 on organic surfaces is proposed here as a major HONO source in London. However, the
4 exact identification of the organics adsorbed on the urban surfaces (humic acids, organic
5 grime, etc.) is out of the scope of the present study. In Sörgel et al. 2011b, it was shown that
6 the results presented by Stemmler et al., 2007 on an artificial humic acid are not able to
7 describe their field observation. The heterogeneous NO_2 uptake kinetics and HONO yields of
8 real urban organic substrates are not known and maybe different compared to the artificial
9 surfaces studied in the laboratory. Detailed laboratory studies on real surfaces collected from
10 the surrounding of the field site in London would be necessary, which is again out of the
11 scope of this study.

12 It should also be pointed out that our model only represents the situation at the measurement
13 height of HONO and the supporting species (5 m) and is not used to attempt to describe the
14 entire boundary layer. Numerous measurements demonstrate that near-surface vertical
15 structure in HONO can be significant at night and during the day (Stutz et al., 2002;
16 Kleffmann, 2003; 2007; Zhang et al., 2009; Villena et al., 2011; Wong et al., 2012; Young et
17 al., 2012; Oswald et al., 2015) and that a model using a near-surface source distributed
18 throughout the boundary layer produces results inconsistent with observations (Vandenboer et
19 al., 2013; Wong et al., 2013; Kim et al., 2014; Sörgel et al., 2015). Thus, some of the
20 discrepancy between the model and measurements, particularly in the early morning when
21 thermal inversions can persist, could be ascribed to biases from vertical stratification in
22 HONO. It is, however, clear that at the present urban background site close to central London
23 and within 5 meters of the surface, a significant missing source of HONO is active when
24 compared to the output of a box model containing most known sources. We suggest from our
25 analysis of the supporting data that processes responsible for the unknown source of HONO
26 in this particular study are at least partially connected with light, NO_2 and organic matter
27 (represented by $k(\text{OH})$), in agreement with the source described in Stemmler et al. (2006;
28 2007).

4.3 HONO contribution to atmospheric oxidation

HONO is known to be an important initiation source of OH radicals (Ren et al., 2003; Ren et al., 2006; Dusanter et al., 2009; Elshorbany et al., 2009; Hofzumahaus et al., 2009; Villena et al., 2011; Michoud et al., 2012; Michoud et al., 2014), so any extra source that is not well understood or defined in models could have a potentially important impact on atmospheric oxidation capacity and hence O₃ and secondary organic aerosol (SOA) production. The model described above was used to produce a rate of production analysis (ROPA) for OH radicals during the measurements campaign, with a view to assessing the importance of HONO and in particular the missing HONO source. It should again be pointed out here that any conclusions drawn from this analysis are only valid for this particular measurement site (i.e. close to the surface). The model is only being used to understand OH production at the HONO measurement height even though the chemistry is taking place in a dynamic boundary layer. For the analysis of the vertical structure of the HONO contribution to the OH initiation, our measurement data is not sufficient and further gradient studies would be necessary. We also do not include the enhanced reactive conversion of NO₂ on other surfaces nor increased direct emissions described in the sensitivity analysis in this investigation.

For this analysis, the ROPA output was plotted for all OH radical sources and the diurnal average for these is shown in figure 10. Initially ignoring the missing HONO source, it can be seen that in the early morning shortly after sunrise, HONO is a significant OH source (30 – 40% of the total, second only to the propagation source of NO + HO₂). This is due to the build-up of HONO concentrations overnight, followed by its rapid photolysis after sunrise. Then, approaching solar noon, whilst the absolute production rate from HONO photolysis remains relatively constant, the dominant OH source becomes the HO₂ + NO reaction. At solar noon, HONO unconstrained in the model accounts for around 40% of the total OH radical sources and 57% of the HO_x initiation sources. During the late afternoon and evening approaching sunset, OH from HONO photolysis again becomes comparable to HO₂ + NO. The photolysis of O₃ is only a minor component of the total OH radical sources throughout the day, peaking at around 10% in early afternoon. The same holds for the ozonolysis of alkenes which is caused, at least in part, by the low levels of measured alkenes. With the model constrained to the measured HONO, it was possible to add on the effect of the missing HONO source to OH radical production rate to the diurnal profile. It can clearly be seen that the OH production rate is significantly increased during the daytime, especially during the

afternoon when constraining the model to measured HONO, where the OH production rate increases by around 20%. This result shows that, even when all currently known sources of HONO are added to a box model, missing HONO sources are still crucial to HO_x radical production at the surface, which is directly relevant to atmospheric oxidation capacity and O₃ formation.

This importance is also shown when the model is used to calculate OH concentrations, as shown in figure 11. If the model is run with PSS calculated HONO (i.e. only OH + NO as a source), there is a significant under prediction of OH levels (~40% during daytime). When the known or postulated HONO sources are included in the model, the predicted OH is increased by a factor of 1.4 – 1.6 during the day. However, during the afternoon, predicted OH is still 20 – 30% lower than modelled, suggesting a missing OH source. It is only when the model is constrained to measured HONO the agreement between measured and modelled OH becomes good (<5% discrepancy at midday and during most of the afternoon) and within the experimental error of the measurements (~15%). This clearly demonstrates the need for models to include accurate HONO data (either from measurements or a model containing all HONO sources and sinks) and thus shows the need for further investigation on the missing HONO source to be carried out.

5 Summary and Conclusions

In this study a month long time series of HONO levels at an urban background site in London was measured, with average mixing ratios showing a peak in the early morning of ~0.6 ppbV and a minimum during early afternoon of ~0.18 ppbV. Analysis of the HONO / NO_x ratio showed a significant secondary peak during daytime, suggesting additional sources of HONO other than the reaction between NO and OH. The presence of a large range of other atmospheric gas and aerosol measurements (including OH and HO₂ radicals), allowed a detailed study of known and postulated production routes of HONO to be undertaken, using both a simple PSS analysis and a box model based on the MCMv3.2. The calculated HONO shows a daytime underestimation of ~0.2 ppbV on average, even when recently suggested sources such as the reaction of HO₂×H₂O with NO₂ to produce HONO, photolysis of adsorbed HNO₃, photo-enhanced conversion of NO₂ on ground and aerosol surfaces and direct traffic emissions are included, again suggesting a significant missing HONO source. Correlation plots of the missing HONO production rate against various other species measured at the site show a reasonable correlation with the product of $j(\text{NO}_2)$ with NO₂ and $k(\text{OH})$, suggesting

1 that the proposed photosensitized heterogeneous conversion of NO_2 to HONO on organic
2 substrates as observed in laboratory studies may be enhanced under these urban conditions.

3 The effect of the missing source of HONO to the oxidising capacity of the urban background
4 atmosphere has been investigated using radical rate of production analyses. These show that
5 OH radical production during the day increases by over 20% if measured HONO is used in
6 the model as compared to allowing the model to run unconstrained to HONO, even with
7 known and postulated HONO sources included. In addition, modelled OH only reproduces the
8 measurement when HONO was constrained in the model. Whilst our results are only valid at
9 the surface due to the likely HONO gradients, it is still an important result and demonstrates
10 the need of a full understanding of the HONO production processes in an urban area such as
11 London in, for example, air quality prediction models. The results presented here provide
12 further evidence that unknown sources of HONO are present in the urban environment, and
13 they are probably a function of NO_x and sunlight. It is not possible to conclude exactly the
14 origin of the source from this work, hence further field measurements and, probably more
15 crucially, laboratory studies are needed to investigate these important processes further.

17 **Acknowledgements**

18 The authors would like to thank the staff and governors of The Sion Manning RC School,
19 North Kensington, London for hosting the field campaign. Thanks also go to Brian Bandy
20 from the University of East Anglia for HCHO and Janet Barlow and Christoforos Halios from
21 the University of Reading for boundary layer height data. The work was funded through the
22 UK Natural Environment Research Council (NERC) ClearfLo project (grant number
23 NE/H003223/1).

1 **References**

- 2 Acker, K., Möller, D., Wieprecht, W., Meixner, F. X., Bohn, B., Gilge, S., Plass-Dülmer, C.,
3 and Berresheim, H.: Strong daytime production of OH from HNO₂ at a rural mountain site,
4 Geophys. Res. Lett., 33, L02809, 10.1029/2005gl024643, 2006.
- 5 Alicke, B., Platt, U., and Stutz, J.: Impact of nitrous acid photolysis on the total hydroxyl
6 radical budget during the Limitation of Oxidant Production/Pianura Padana Produzione di
7 Ozono study in Milan, J. Geophys. Res., 107, 8196, 10.1029/2000jd000075, 2002.
- 8 Arens, F., L. Gutzwiller, U. Baltensperger, H. W. Gäggeler, and M. Ammann: Heterogeneous
9 Reaction of NO₂ on Diesel Soot Particles, Environ. Sci. Technol., 35, 2191-2199, 2001.
- 10 Atkinson, R., Baulch, D. L., Cox, R. A., Crowley, J. N., Hampson, R. F., Hynes, R. G.,
11 Jenkin, M. E., Rossi, M. J., and Troe, J.: Evaluated kinetic and photochemical data for
12 atmospheric chemistry: Volume I - gas phase reactions of O_x, HO_x, NO_x and SO_x species,
13 Atmos. Chem. Phys., 4, 1461-1738, 10.5194/acp-4-1461-2004, 2004.
- 14 Barlow, J. F., Dunbar, T. M., Nemitz, E. G., Wood, C. R., Gallagher, M. W., Davies, F.,
15 O'Connor, E., and Harrison, R. M.: Boundary layer dynamics over London, UK, as observed
16 using Doppler lidar during REPARTEE-II, Atmos. Chem. Phys., 11, 2111-2125, 10.5194/acp-
17 11-2111-2011, 2011.
- 18 Barlow, J. F., Halios, C. H., Lane, S. E., and Wood, C. R.: Observations of urban boundary
19 layer structure during a strong urban heat island event, Environ. Fluid Mech., 15(2), 373-398,
20 10.1007/s10652-014-9335-6, 2015.
- 21 Bejan, I., Abd El Aal, Y., Barnes, I., Benter, T., Bohn, B., Wiesen, P., and Kleffmann, J.: The
22 photolysis of ortho-nitrophenols: a new gas phase source of HONO, Phys. Chem. Chem.
23 Phys., 8, 2028-2035, 10.1039/b516590c, 2006.
- 24 Bigi, A., and Harrison, R. M.: Analysis of the air pollution climate at a central urban
25 background site, Atmos. Environ., 44, 2004-2012, 10.1016/j.atmosenv.2010.02.028, 2010.
- 26 Bohnenstengel, S. I., Belcher, S. E., Aiken, A., Allan, J. D., Allen, G., Bacak, A., Bannan, T.
27 J., Barlow, J. F., Beddows, D. C. S., Bloss, W. J., Booth, A. M., Chemel, C., Coceal, O., Di
28 Marco, C. F., Dubey, M. K., Faloon, K. H., Fleming, Z. L., Furger, M., Gietl, J. K., Graves,
29 R. R., Green, D. C., Grimmond, C. S. B., Halios, C. H., Hamilton, J. F., Harrison, R. M.,
30 Heal, M. R., Heard, D. E., Helfter, C., Herndon, S. C., Holmes, R. E., Hopkins, J. R., Jones,

1 A. M., Kelly, F. J., Kotthaus, S., Langford, B., Lee, J. D., Leigh, R. J., Lewis, A. C., Lidster,
2 R. T., Lopez-Hilfiker, F. D., McQuaid, J. B., Mohr, C., Monks, P. S., Nemitz, E., Ng, N. L.,
3 Percival, C. J., Prévôt, A. S. H., Ricketts, H. M. A., Sokhi, R., Stone, D., Thornton, J. A.,
4 Tremper, A. H., Valach, A. C., Visser, S., Whalley, L. K., Williams, L. R., Xu, L., Young, D.
5 E., and Zotter, P.: Meteorology, air quality, and health in London: The ClearfLo project, B.
6 Am. Meteorol. Soc., online, 10.1175/BAMS-D-12-00245.1, 2014.

7 Bush, T. J., Tsagatakis, I., King, K., and Passant, N. R.: NAEI UK Emission Mapping
8 Methodology 2006, AEATY/ENV/R/2696, available at: <http://www.naei.org.uk/reoprts.php>,
9 2006.

10 Cappa, C. D., Onasch, T. B., Massoli, P., Worsnop, D. R., Bates, T. S., Cross, E. S.,
11 Davidovits, P., Hakala, J., Hayden, K. L., Jobson, B. T., Kolesar, K. R., Lack, D. A., Lerner,
12 B. M., Li, S.-M., Mellon, D., Nuaaman, I., Olfert, J. S., Petäjä, T., Quinn, P. K., Song, C.,
13 Subramanian, R., Williams, E. J., and Zaveri, R. A.: Radiative Absorption Enhancements Due
14 to the Mixing State of Atmospheric Black Carbon, *Science*, 337, 1078-1081,
15 10.1126/science.1223447, 2012.

16 Creasey, D. J., Heard, D. E., and Lee, J. D.: Absorption cross-section measurements of water
17 vapour and oxygen at 185 nm. Implications for the calibration of field instruments to measure
18 OH, HO₂ and RO₂ radicals, *Geophys. Res. Lett.*, 27, 1651-1654, 10.1029/1999gl011014,
19 2000.

20 Dentener, F., Williams, J., and Metzger, S.: Aqueous phase reaction of HNO₄: The impact on
21 tropospheric chemistry, *J. Atmos. Chem.*, 41, 109-134, 10.1023/a:1014233910126, 2002.

22 Dransfield, T. J., Donahue, N. M., and Anderson, J. G.: High-Pressure Flow Reactor Product
23 Study of the Reactions of HO_x + NO₂: The Role of Vibrationally Excited Intermediates†, *J.*
24 *Phys. Chem. A*, 105, 1507-1514, 10.1021/jp002391+, 2001.

25 Drummond, J. W., Volz, A., and Ehhalt, D. H.: An Optimized Chemiluminescence Detector
26 for Tropospheric NO Measurements, *J. Atmos. Chem.*, 2, 287-306, 10.1007/bf00051078,
27 1985.

28 Dusanter, S., Vimal, D., Stevens, P. S., Volkamer, R., Molina, L. T., Baker, A., Meinardi, S.,
29 Blake, D., Sheehy, P., Merten, A., Zhang, R., Zheng, J., Fortner, E. C., Junkermann, W.,
30 Dubey, M., Rahn, T., Eichinger, B., Lewandowski, P., Prueger, J., and Holder, H.:

1 Measurements of OH and HO₂ concentrations during the MCMA-2006 field campaign - Part
2 2: Model comparison and radical budget, *Atmos. Chem. Phys.*, 9, 6655-6675, 2009.

3 Edwards, G. D., and Monks, P. S.: Performance of a single-monochromator diode array
4 spectroradiometer for the determination of actinic flux and atmospheric photolysis
5 frequencies, *J. Geophys. Res.*, 108, 2003.

6 Elshorbany, Y. F., Kurtenbach, R., Wiesen, P., Lissi, E., Rubio, M., Villena, G., Gramsch, E.,
7 Rickard, A. R., Pilling, M. J., and Kleffmann, J.: Oxidation capacity of the city air of
8 Santiago, Chile, *Atmos. Chem. Phys.*, 9, 2257-2273, 2009.

9 Forster, G. L., Sturges, W. T., Fleming, Z. L., Bandy, B. J., and Emeis, S.: A year of H₂
10 measurements at Weybourne Atmospheric Observatory, UK, 2012, *Tellus B*, 64, 17771,
11 10.3402/tellusb.v64i0.17771, 2012.

12 George, C., Strekowski, R. S., Kleffmann, J., Stemmler, K., and Ammann, M.:
13 Photoenhanced uptake of gaseous NO₂ on solid organic compounds: a photochemical source
14 of HONO?, *Faraday Discuss.*, 130, 195-210, 10.1039/b417888m, 2005.

15 Harrison, R. M. and Kitto, A.-M. N.: Evidence for a Surface Source of Atmospheric Nitrous
16 Acid, *Atmos. Environ.*, 28, 1089-1094, 1994.

17 Heland, J., Kleffmann, J., Kurtenbach, R., and Wiesen, P.: A New Instrument To Measure
18 Gaseous Nitrous Acid (HONO) in the Atmosphere, *Environ. Sci. Technol.*, 35, 3207-3212,
19 10.1021/es000303t, 2001.

20 Hofzumahaus, A., Rohrer, F., Lu, K. D., Bohn, B., Brauers, T., Chang, C. C., Fuchs, H.,
21 Holland, F., Kita, K., Kondo, Y., Li, X., Lou, S., Shao, M., Zeng, L., Wahner, A., and Zhang,
22 Y.: Amplified Trace Gas Removal in the Troposphere, *Science*, 324, 1702-1704, 2009.

23 Hofzumahaus, A: Oral presentation during the conference: Atmospheric Chemical
24 Mechanisms “Simple Models – Real World Complexities” December, 10-12, 2014, UC
25 Davis.

26 Hopkins, J. R., Lewis, A. C., and Read, K. A.: A two-column method for long-term
27 monitoring of non-methane hydrocarbons (NMHCs) and oxygenated volatile organic
28 compounds (o-VOCs), *J. Environ. Monit.*, 5, 8-13, 2003.

29 Jenkin, M. E., Wyche, K. P., Evans, C. J., Carr, T., Monks, P. S., Alfarra, M. R., Barley, M.
30 H., McFiggans, G. B., Young, J. C., and Rickard, A. R.: Development and chamber

1 evaluation of the MCM v3.2 degradation scheme for beta-caryophyllene, *Atmos. Chem.*
2 *Phys.*, 12, 5275-5308, 10.5194/acp-12-5275-2012, 2012.

3 Joyce, P. L., von Glasow, R., and Simpson, W. R.: The fate of NO_x emissions due to
4 nocturnal oxidation at high latitudes: 1-D simulations and sensitivity experiments, *Atmos.*
5 *Chem. Phys.*, 14, 7601-7616, 10.5194/acp-14-7601-2014, 2014.

6 Kim, S., Vandenboer, T. C., Young, C. J., Riedel, T. P., Thornton, J. A., Swarthout, B., Sive,
7 B., Lerner, B., Gilman, J. B., Warneke, C., Roberts, J. M., Guenther, A. B., Wagner, N. L.,
8 Dubé, W. P., Williams, E. and Brown, S. S.: The primary and recycling sources of OH during
9 the NACHT-2011 campaign: HONO as an important OH primary source in the wintertime, *J.*
10 *Geophys. Res.*, 119, 6886–6896, doi:10.1002/2013JD020225, 2014.

11 Kleffmann, J., K. H. Becker, M. Lackhoff, and P. Wiesen: Heterogeneous Conversion of NO₂
12 on Carbonaceous Surfaces, *Phys. Chem. Chem. Phys.*, 1, 5443-5450, 1999.

13 Kleffmann, J., R. Kurtenbach, J. Lörzer, P. Wiesen, N. Kalthoff, B. Vogel, and H. Vogel:
14 Measured and Simulated Vertical Profiles of Nitrous Acid, Part I: Field Measurements,
15 *Atmos. Environ.*, 37, 2949-2955, 2003.

16 Kleffmann, J., Gavriloaiei, T., Hofzumahaus, A., Holland, F., Koppmann, R., Rupp, L.,
17 Schlosser, E., Siese, M., and Wahner, A.: Daytime formation of nitrous acid: A major source
18 of OH radicals in a forest, *Geophys. Res. Lett.*, 32, L05818, 10.1029/2005gl022524, 2005.

19 Kleffmann, J., Lörzer, J. C., Wiesen, P., Kern, C., Trick, S., Volkamer, R., Rodenas, M., and
20 Wirtz, K.: Intercomparison of the DOAS and LOPAP techniques for the detection of nitrous
21 acid (HONO), *Atmos. Environ.*, 40, 3640-3652, 10.1016/j.atmosenv.2006.03.027, 2006.

22 Kleffmann, J.: Daytime sources of nitrous acid (HONO) in the atmospheric boundary layer,
23 *Chem. Phys. Chem.*, 8, 1137-1144, 10.1002/cphc.200700016, 2007.

24 Kraus, A., and Hofzumahaus, A.: Field measurements of atmospheric photolysis frequencies
25 for O₃, NO₂, HCHO, CH₃CHO, H₂O₂, and HONO by UV spectroradiometry, *J. Atmos.*
26 *Chem.*, 31, 161-180, 10.1023/a:1005888220949, 1998.

27 Kurtenbach, R., Becker, K. H., Gomes, J. A. G., Kleffmann, J., Lörzer, J. C., Spittler, M.,
28 Wiesen, P., Ackermann, R., Geyer, A., and Platt, U.: Investigations of emissions and
29 heterogeneous formation of HONO in a road traffic tunnel, *Atmos. Environ.*, 35, 3385-3394,
30 10.1016/s1352-2310(01)00138-8, 2001.

1 Lee, J. D., Moller, S. J., Read, K. A., Lewis, A. C., Mendes, L., and Carpenter, L. J.: Year-
2 round measurements of nitrogen oxides and ozone in the tropical North Atlantic marine
3 boundary layer, *J. Geophys. Res.*, 114, D21302, 10.1029/2009jd011878, 2009.

4 Lee, B. H., Wood, E. C., Herndon, S. C., Lefer, B. L., Luke, W. T., Brune, W. H., Nelson, D.
5 D., Zahniser, M. S., and Munger, J. W.: Urban measurements of atmospheric nitrous acid: A
6 caveat on the interpretation of the HONO photostationary state, *J. Geophys. Res. Atmos.*, 118,
7 10.1002/2013JD020341, 2013.

8 Legrand, M., Preunkert, S., Frey, M., Bartels-Rausch, T., Kukui, A., King, M. D., Savarino,
9 J., Kerbrat, M., and Jourdain, B.: Large mixing ratios of atmospheric nitrous acid (HONO) at
10 Concordia (East Antarctic Plateau) in summer: a strong source from surface snow?, *Atmos.*
11 *Chem. Phys.*, 14, 9963-9976, 10.5194/acp-14-9963-2014, 2014.

12 Levy II, H.: Normal Atmosphere: Large Radical and Formaldehyde Concentrations Predicted,
13 *Science*, 173, 141-143, 1971.

14 Li, S., Matthews, J., and Sinha, A.: Atmospheric hydroxyl radical production from
15 electronically excited NO₂ and H₂O, *Science*, 319, 1657-1660, 10.1126/science.1151443,
16 2008.

17 Li, X., Rohrer, F., Hofzumahaus, A., Brauers, T., Häseler, R., Bohn, B., Broch, S., Fuchs, H.,
18 Gomm, S., Holland, F., Jäger, J., Kaiser, J., Keutsch, F. N., Lohse, I., Lu, K., Tillmann, R.,
19 Wegener, R., Wolfe, G. M., Mentel, T. F., Kiendler-Scharr, A., and Wahner, A.: Missing Gas-
20 Phase Source of HONO Inferred from Zeppelin Measurements in the Troposphere, *Science*,
21 344, 292-296, 10.1126/science.1248999, 2014.

22 Lidster, R. T., Hamilton, J. F., Lee, J. D., Lewis, A. C., Hopkins, J. R., Punjabi, S., Rickard,
23 A. R., and Young, J. C.: The impact of monoaromatic hydrocarbons on OH reactivity in the
24 coastal UK boundary layer and free troposphere, *Atmos. Chem. Phys.*, 14, 6677-6693,
25 10.5194/acp-14-6677-2014, 2014.

26 Michoud, V., Kukui, A., Camredon, M., Colomb, A., Borbon, A., Miet, K., Aumont, B.,
27 Beekmann, M., Durand-Jolibois, R., Perrier, S., Zapf, P., Siour, G., Ait-Helal, W., Locoge,
28 N., Sauvage, S., Afif, C., Gros, V., Furger, M., Ancellet, G., and Doussin, J. F.: Radical
29 budget analysis in a suburban European site during the MEGAPOLI summer field campaign,
30 *Atmos. Chem. Phys.*, 12, 11951-11974, 10.5194/acp-12-11951-2012, 2012.

1 Michoud, V., Colomb, A., Borbon, A., Miet, K., Beekmann, M., Camredon, M., Aumont, B.,
2 Perrier, S., Zapf, P., Siour, G., Ait-Helal, W., Afif, C., Kukui, A., Furger, M., Dupont, J. C.,
3 Haeffelin, M., and Doussin, J. F.: Study of the unknown HONO daytime source at a European
4 suburban site during the MEGAPOLI summer and winter field campaigns, *Atmos. Chem.*
5 *Phys.*, 14, 2805-2822, 10.5194/acp-14-2805-2014, 2014.

6 Monge, M. E., D'Anna, B., Mazri, L., Giroir-Fendler, A., Ammann, M., Donaldson, D. J., and
7 George, C.: Light changes the atmospheric reactivity of soot, *Proc. Natl. Acad. Sci. U.S.A.*,
8 107, 6605-6609, 10.1073/pnas.0908341107, 2010.

9 Oswald R., Behrendt, T., Ermel, M., Wu, D., Su, H., Cheng, Y., Breuninger, C., Moravek, A.,
10 Mougin, E., Delon, C., Loubet, B., Pommerening-Röser, A., Sörgel, M., Pöschl, U.,
11 Hoffmann, T., Andreae, M. O., Meixner, F. X., and Trebs, I.: HONO Emissions from Soil
12 Bacteria as a Major Source of Atmospheric Reactive Nitrogen, *Science*, 341, 1233-1235,
13 2013.

14 Oswald, R., Ermel, M., Hens, K., Novelli, A., Ouwersloot, H. G., Paasonen, P., Petäjä, T.,
15 Sipilä, M., Keronen, P., Bäck, J., Königstedt, R., Hosaynali Beygi, Z., Fischer, H., Bohn, B.,
16 Kubistin, D., Harder, H., Martinez, M., Williams, J., Hoffmann, T., Trebs, I. and Sörgel, M.:
17 Comparison of HONO budgets for two measurement heights at a field station within the
18 boreal forest in Finland, *Atmos. Chem. Phys.*, 15, 799–813, doi:10.5194/acp-15-799-2015,
19 2015.

20 Pollack, I. B., Lerner, B. M., and Ryerson, T. B.: Evaluation of ultraviolet light-emitting
21 diodes for detection of atmospheric NO₂ by photolysis - chemiluminescence, *J. Atmos.*
22 *Chem.*, 65, 111-125, 10.1007/s10874-011-9184-3, 2010.

23 Qin, M., Xie, P., Su, H., Gu, J., Peng, F., Li, S., Zeng, L., Liu, J., Liu, W., and Zhang, Y.: An
24 observational study of the HONO-NO₂ coupling at an urban site in Guangzhou City, South
25 China, *Atmos. Environ.*, 43, 5731-5742, 10.1016/j.atmosenv.2009.08.017, 2009.

26 Ren, X. R., Harder, H., Martinez, M., Leshner, R. L., Oliger, A., Simpas, J. B., Brune, W. H.,
27 Schwab, J. J., Demerjian, K. L., He, Y., Zhou, X., and Gao, H.: OH and HO₂ chemistry in the
28 urban atmosphere of New York City, *Atmos. Environ.*, 37, 3639-3651, 2003.

29 Ren, X., Brune, W. H., Oliger, A., Metcalf, A. R., Simpas, J. B., Shirley, T., Schwab, J. J.,
30 Bai, C. H., Roychowdhury, U., Li, Y. Q., Cai, C. X., Demerjian, K. L., He, Y., Zhou, X. L.,
31 Gao, H. L., and Hou, J.: OH, HO₂, and OH reactivity during the PMTACS-NY Whiteface

1 Mountain 2002 campaign: Observations and model comparison, *J. Geophys. Res.*, 111,
2 D10S03, 10.1029/2005JD006126, 2006.

3 Ren, X., Sanders, J. E., Rajendran, A., Weber, R. J., Goldstein, A. H., Pusede, S. E., Browne,
4 E. C., Min, K.-E., and Cohen, R. C.: A relaxed eddy accumulation system for measuring
5 vertical fluxes of nitrous acid, *Atmos. Meas. Tech.*, 4, 2093–2103, 10.5194/amt-4-2093-2011,
6 2011.

7 Rutter, A. P., Malloy, Q. G. J., Leong, Y. J., Gutierrez, C. V., Calzada, M., Scheuer, E., Dibb,
8 J. E. and Griffin, R. J.: The reduction of HNO_3 by volatile organic compounds emitted by
9 motor vehicles, *Atmos. Environ.*, 48, 200–206, doi:10.1016/j.atmosenv.2014.01.056, 2014.

10 Salmon, R. A., Bauguitte, S. J. B., Bloss, W., Hutterli, M. A., Jones, A. E., Read, K., and
11 Wolff, E. W.: Measurement and interpretation of gas phase formaldehyde concentrations
12 obtained during the CHABLIS campaign in coastal Antarctica, *Atmos. Chem. Phys.*, 8, 4085-
13 4093, 10.5194/acp-8-4085-2008, 2008.

14 Sander, S. P., and Peterson, M. E.: Kinetics of the Reaction $\text{HO}_2 + \text{NO}_2 + \text{M} = \text{HO}_2\text{NO}_2 + \text{M}$, *J.*
15 *Phys. Chem.*, 88, 1566-1571, 10.1021/j150652a025, 1984.

16 Scharko, N. K., Berke, A. E. and Raff, J. D.: Release of Nitrous Acid and Nitrogen Dioxide
17 from Nitrate Photolysis in Acidic Aqueous Solutions, *Environ. Sci. Technol.*, **48**, 11991-
18 12001, doi:10.1021/es503088x, 2014.

19 Sörgel, M., Trebs, I., Serafimovich, A., Moravek, A., Held, A. and Zetzsch, C.: Simultaneous
20 HONO measurements in and above a forest canopy: Influence of turbulent exchange on
21 mixing ratio differences, *Atmos. Chem. Phys.*, 11(2), 841–855, doi:10.5194/acp-11-841-2011,
22 2011a.

23 Sörgel, M., Regelin, E., Bozem, H., Diesch, J.-M., Drewnick, F., Fischer, H., Harder, H.,
24 Held, A., Hosaynali-Beygi, Z., Martinez, M. and Zetzsch, C.: Quantification of the unknown
25 HONO daytime source and its relation to NO_2 , *Atmos. Chem. Phys.*, 11(20), 10433–10447,
26 doi:10.5194/acp-11-10433-2011, 2011b.

27 Sörgel, M., Trebs, I., Wu, D. and Held, A.: A comparison of measured HONO uptake and
28 release with calculated source strengths in a heterogeneous forest environment, *Atmos. Chem.*
29 *Phys.*, 15(16), 9237–9251, doi:10.5194/acp-15-9237-2015, 2015.

1 Steinbacher, M., Zellweger, C., Schwarzenbach, B., Bugmann, S., Buchmann, B., Ordonez,
2 C., Prevot, A. S. H., and Hueglin, C.: Nitrogen oxide measurements at rural sites in
3 Switzerland: Bias of conventional measurement techniques, *J. Geophys. Res.*, 112, D11307,
4 10.1029/2006jd007971, 2007.

5 Stemmler, K., Ammann, M., Donders, C., Kleffmann, J., and George, C.: Photosensitized
6 reduction of nitrogen dioxide on humic acid as a source of nitrous acid, *Nature*, 440, 195-198,
7 10.1038/nature04603, 2006.

8 Stemmler, K., Ndour, M., Elshorbany, Y., Kleffmann, J., D'Anna, B., George, C., Bohn, B.,
9 and Ammann, M.: Light induced conversion of nitrogen dioxide into nitrous acid on
10 submicron humic acid aerosol, *Atmos. Chem. Phys.*, 7, 4237-4248, 2007.

11 Stone, D. and Rowley, D. M., Kinetics of the Gas Phase HO₂ Self-Reaction: Effects of
12 Temperature, Pressure, Water and Methanol Vapours, *Phys. Chem. Chem. Phys.*, 7, 2156 –
13 2163, 2005.

14 Stutz, J., Alicke, B., and Neftel, A.: Nitrous acid formation in the urban atmosphere: Gradient
15 measurements of NO₂ and HONO over grass in Milan, Italy, *J. Geophys. Res.*, 107, 8192,
16 10.1029/2001jd000390, 2002.

17 Su, H., Cheng, Y. F., Cheng, P., Zhang, Y. H., Dong, S., Zeng, L. M., Wang, X., Slanina, J.,
18 Shao, M., and Wiedensohler, A.: Observation of nighttime nitrous acid (HONO) formation at
19 a non-urban site during PRIDE-PRD2004 in China, *Atmos. Environ.*, 42, 6219-6232,
20 10.1016/j.atmosenv.2008.04.006, 2008a.

21 Su, H., Cheng, Y. F., Shao, M., Gao, D. F., Yu, Z. Y., Zeng, L. M., Slanina, J., Zhang, Y. H.,
22 and Wiedensohler, A.: Nitrous acid (HONO) and its daytime sources at a rural site during the
23 2004 PRIDE-PRD experiment in China, *J. Geophys. Res. Atmos.*, 113, D14312,
24 10.1029/2007jd009060, 2008b.

25 Su, H., Cheng, Y., Oswald, R., Behrendt, T., Trebs, I., Meixner, F. X., Andreae, M. O.,
26 Cheng, P., Zhang, Y., and Pöschl, U.: Soil Nitrite as a Source of Atmospheric HONO and OH
27 Radicals, *Science*, 333, 1616-1618, 10.1126/science.1207687, 2011.

28 Trebs, I., Lara, L. L., Zeri, L. M. M., Gatti, L. V., Artaxo, P., Slanina, J., Andreae, M. O., and
29 Meixner, F. X.: Dry and wet deposition of inorganic nitrogen compounds to a tropical pasture
30 site (Rondonia, Brazil), *Atmos. Chem. Phys.*, 6, 447–469, 2006.

1 Tyndall, G. S., Orlando, J. J., and Calvert, J. G.: Upper Limit for the Rate Coefficient for the
2 Reaction $\text{HO}_2 + \text{NO}_2 \rightarrow \text{HONO} + \text{O}_2$, *Environ. Sci. Technol.*, 29, 202-206,
3 10.1021/es00001a026, 1995.

4 VandenBoer, T. C., Brown, S. S., Murphy, J. G., Keene, W. C., Young, C. J., Pszenny, A. A.
5 P., Kim, S., Warneke, C., de Gouw, J. A., Maben, J. R., Wagner, N. L., Riedel, T. P.,
6 Thornton, J. A., Wolfe, D. E., Dubé, W. P., Öztürk, F., Brock, C. A., Grossberg, N., Lefer, B.,
7 Lerner, B., Middlebrook, A. M., and Roberts, J. M.: Understanding the role of the ground
8 surface in HONO vertical structure: High resolution vertical profiles during NACHTT-11, *J.*
9 *Geophys. Res.*, 118, 10,155–10,171, doi:10.1002/jgrd.50721, 2013.

10 VandenBoer, T. C., Young, C. J., Talukdar, R. K., Markovic, M. Z., Brown, S. S., Roberts, J.
11 M. and Murphy, J. G.: Nocturnal loss and daytime source of nitrous acid through reactive
12 uptake and displacement, *Nature Geosci.*, 8(1), 55–60, doi:10.1038/ngeo2298, 2015.

13 Villena, G., Kleffmann, J., Kurtenbach, R., Wiesen, P., Lissi, E., Rubio, M. A., Croxatto, G.,
14 and Rappenglück, B.: Vertical gradients of HONO, NO_x and O_3 in Santiago de Chile, *Atmos.*
15 *Environ.*, 45, 3867-3873, 10.1016/j.atmosenv.2011.01.073, 2011.

16 Villena, G., Bejan, I., Kurtenbach, R., Wiesen, P., and Kleffmann, J.: Interferences of
17 commercial NO_2 instruments in the urban atmosphere and in a smog chamber, *Atmos. Meas.*
18 *Tech.*, 5, 149-159, 10.5194/amt-5-149-2012, 2012.

19 Vogel, B., Vogel, H., Kleffmann, J. and Kurtenbach, R.: Measured and simulated vertical
20 profiles of nitrous acid - Part II. Model simulations and indications for a photolytic source,
21 *Atmos. Environ.*, 37(21), 2957–2966, doi:10.1016/S1352-2310(03)00243-7, 2003.

22 Whalley, L. K., Blitz, M. A., Desservettaz, M., Seakins, P. W., and Heard, D. E.: Reporting
23 the sensitivity of laser-induced fluorescence instruments used for HO_2 detection to an
24 interference from RO_2 radicals and introducing a novel approach that enables HO_2 and certain
25 RO_2 types to be selectively measured, *Atmos. Meas. Tech.*, 6, 3425-3440, 10.5194/amt-6-
26 3425-2013, 2013.

27 Whalley, L. K., Stone, D., George, I. J., Mertes, S., van Pinxteren, D., Tilgner, A., Herrmann,
28 H., Evans, M. J., and Heard, D. E.: The influence of clouds on radical concentrations:
29 observations and modelling studies of HO_x during the Hill Cap Cloud Thuringia (HCCT)
30 campaign in 2010, *Atmos. Chem. Phys.*, 15, 3289-3301, 2015a.

1 Whalley, L. K., Stone, D., Bandy, B., Dunmore, R., Hamilton, J. F., Hopkins, J. R., Lee, J. D.,
2 Lewis, A. C., and Heard, D. E., Atmospheric OH reactivity in central London: observations,
3 model predictions and estimates of in situ ozone production, *Atmos. Chem. Phys. Discuss.*,
4 15, 31247-31286, 2015b.

5 Wong, K. W., Oh, H.-J., Lefer, B. L., Rappenglück, B., and Stutz, J.: Vertical Profiles of
6 Nitrous Acid in the Nocturnal Urban Atmosphere of Houston, TX, *Atmos. Chem. Phys.*, 11,
7 3595-3609, doi:10.5194/acp-11-3595-2011, 2011.

8 Wong, K. W., Tsai, C., Lefer, B., Haman, C., Grossberg, N., Brune, W. H., Ren, X., Luke,
9 W., and Stutz, J.: Daytime HONO vertical gradients during SHARP 2009 in Houston, TX,
10 *Atmos. Chem. Phys.*, 12, 635-652, 10.5194/acp-12-635-2012, 2012.

11 Wong, K. W., Tsai, C., Lefer, B., Grossberg, N. and Stutz, J.: Modeling of daytime HONO
12 vertical gradients during SHARP 2009, *Atmos. Chem. Phys.*, 13(7), 3587–3601,
13 doi:10.5194/acp-13-3587-2013, 2013.

14 Ye, C.; Zhou, X.; Pu, D.; Stutz, J.; Festa, J.; Spolaor, M.; Cantrell, C.; Mauldin, R. L.;
15 Weinheimer, A.; Haggerty, J. Comment on “Missing Gas-phase Source of HONO Inferred
16 from Zeppelin Measurements in the Troposphere”, *Science*, 348, 1326-d, 2015.

17 Young, C. J., Washenfelder, R. A., Roberts, J. M., Mielke, L. H., Osthoff, H. D., Tsai, C.,
18 Pikelnaya, O., Stutz, J., Veres, P. R., Cochran, A. K., Vandenboer, T. C., Flynn, J., Grossberg,
19 N., Haman, C. L., Lefer, B., Stark, H., Graus, M., De Gouw, J., Gilman, J. B., Kuster, W. C.
20 and Brown, S. S.: Vertically resolved measurements of nighttime radical reservoirs in Los
21 Angeles and their contribution to the urban radical budget, *Environ. Sci. Technol.*, 46(20),
22 10965–10973, doi:10.1021/es302206a, 2012.

23 Young, D. E., Allan, J. D., Williams, P. I., Green D. C., Harrison, R. M., Yin, J., Flynn, M. J.,
24 Gallagher, M. W. and Coe, H.: Investigating a two-component model of solid fuel organic
25 aerosol in London: processes, PM1 contributions, and seasonality, *Atmos. Chem. Phys.*, 15,
26 2429-2443, 2015.

27 Zhang, N., Zhou, X., Shepson, P. B., Gao, H., Alaghmand, M. and Stirm, B.: Aircraft
28 measurement of HONO vertical profiles over a forested region, *Geophys. Res. Lett.*, 36(15),
29 L15820, doi:10.1029/2009GL038999, 2009.

30 Zhang, N., Zhou, X., Bertman, S., Tang, D., Alaghmand, M., Shepson, P. B., and Carroll, M.
31 A.: Measurements of ambient HONO concentrations and vertical HONO flux above a

1 northern Michigan forest canopy, *Atmos. Chem. Phys.*, 12, 8285-8296, doi:10.5194/acp-12-
2 8285-2012, 2012

3 Zhou, X., Civerolo, K., Dai, H., Huang, G., Schwab, J., and Demerjian, K.: Summertime
4 nitrous acid chemistry in the atmospheric boundary layer at a rural site in New York State, *J.*
5 *Geophys. Res.*, 107, 4590, 10.1029/2001jd001539, 2002.

6 Zhou, X., Gao, H., He, Y., Huang, G., Bertman, S. B., Civerolo, K., and Schwab, J.: Nitric
7 acid photolysis on surfaces in low-NO_x environments: Significant atmospheric implications,
8 *Geophys. Res. Lett.*, 30, 2217, 10.1029/2003gl018620, 2003.

9 Zhou, X., Zhang, N., TerAvest, M., Tang, D., Hou, J., Bertman, S., Alaghmand, M., Shepson,
10 P. B., Carroll, M. A., Griffith, S., Dusanter, S., and Stevens, P. S.: Nitric acid photolysis on
11 forest canopy surface as a source for tropospheric nitrous acid, *Nature Geoscience*, 4, 440-
12 443, doi:10.1038/NGEO1164, 2011.

13 Ziemba, L. D., Dibb, J. E., Griffin, R. J., Anderson, C. H., Whitlow, S. I., Lefer, B. L.,
14 Rappenglück, B. and Flynn, J.: Heterogeneous conversion of nitric acid to nitrous acid on the
15 surface of primary organic aerosol in an urban atmosphere, *Atmos. Environ.*, 44(33), 4081–
16 4089, doi:10.1016/j.atmosenv.2008.12.024, 2010.

17
18

1 Table 1. Correlation coefficients (r^2) for plots between various species measured during
2 ClearfLo (and their products), using $j(\text{NO}_2)$ as a proxy for radiation, and the missing HONO
3 source from the model (using the model with all additional sources). The species used were
4 chosen using the method described in the text. SA = total aerosol surface area. See
5 supplementary material figure S1 for plots.

| Species | r^2 for correlation vs missing HONO |
|---|---------------------------------------|
| $j(\text{NO}_2)$ | 0.5394 |
| H_2O | 0.0004 |
| NO | 0.0270 |
| NO_2 | 0.0001 |
| Temp | 0.3557 |
| HNO_3 ads. | 0.0966 |
| OH | 0.2745 |
| HO_2 | 0.1925 |
| RO_2 | 0.2763 |
| $k(\text{OH})$ | 0.0001 |
| NO_3^- aero. | 0.0006 |
| NH_4^+ aero. | 0.0007 |
| aerosol surface area (SA) | 0.0001 |
| $j(\text{NO}_2) \times \text{H}_2\text{O}$ | 0.5981 |
| $j(\text{NO}_2) \times \text{NO}_2$ | 0.6960 |
| $j(\text{NO}_2) \times T$ | 0.6276 |
| $j(\text{NO}_2) \times k(\text{OH})$ | 0.6781 |
| $j(\text{NO}_2) \times \text{NH}_4^+$ | 0.5829 |
| $j(\text{NO}_2) \times \text{HNO}_3$ ads. | 0.4356 |
| $\text{H}_2\text{O} \times \text{HNO}_3$ ads. | 0.1044 |
| $\text{H}_2\text{O} \times \text{OH}$ | 0.3378 |
| $\text{H}_2\text{O} \times \text{RO}_2$ | 0.2899 |
| $\text{H}_2\text{O} \times \text{NO}_3^-$ aero. | 0.0006 |
| $\text{NO} \times \text{HNO}_3$ | 0.1276 |
| $\text{NO} \times \text{OH}$ | 0.2791 |
| $\text{NO} \times \text{HO}_2$ | 0.2580 |
| $\text{NO}_2 \times \text{OH}$ | 0.3867 |
| temp $\times \text{OH}$ | 0.3952 |
| $\text{OH} \times k(\text{OH})$ | 0.3497 |
| $\text{OH} \times \text{NH}_4^+$ aero. | 0.3888 |
| $\text{HO}_2 \times k(\text{OH})$ | 0.1941 |
| $\text{RO}_2 \times k(\text{OH})$ | 0.2819 |
| $j(\text{NO}_2) \times \text{NO}_2 \times T$ | 0.7262 |
| $j(\text{NO}_2) \times T \times k(\text{OH})$ | 0.7069 |
| $j(\text{NO}_2) \times \text{NO}_2 \times k(\text{OH})$ | 0.6594 |
| $\text{NO} \times \text{HNO}_3$ ads. $\times \text{OH}$ | 0.4085 |
| $\text{NO} \times \text{HNO}_3$ ads. $\times \text{HO}_2$ | 0.2916 |
| $\text{NO} \times \text{HNO}_3$ ads. $\times \text{RO}_2$ | 0.3198 |
| $j(\text{NO}_2) \times \text{H}_2\text{O} \times T \times k(\text{OH})$ | 0.7280 |

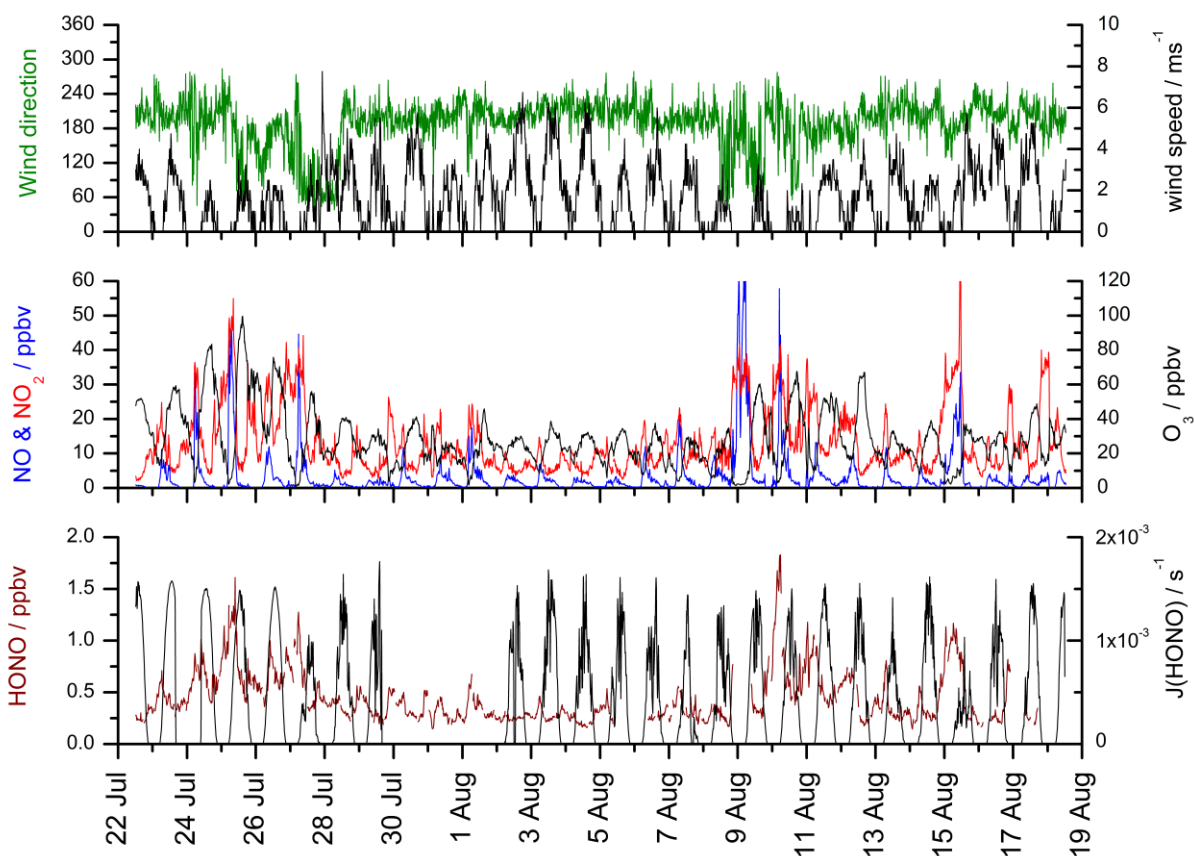


Figure 1. Time series of selected data from the ClearfLo intensive operation period (July and August 2012). The top panel shows wind speed (black) and wind direction (green); the middle panel shows NO (blue), NO₂ (red) and O₃ (black); and the bottom panel shows HONO (dark red) and j(HONO) (black). All data is 15 minute averaged and plotted as UTC (local time - 1 hour).

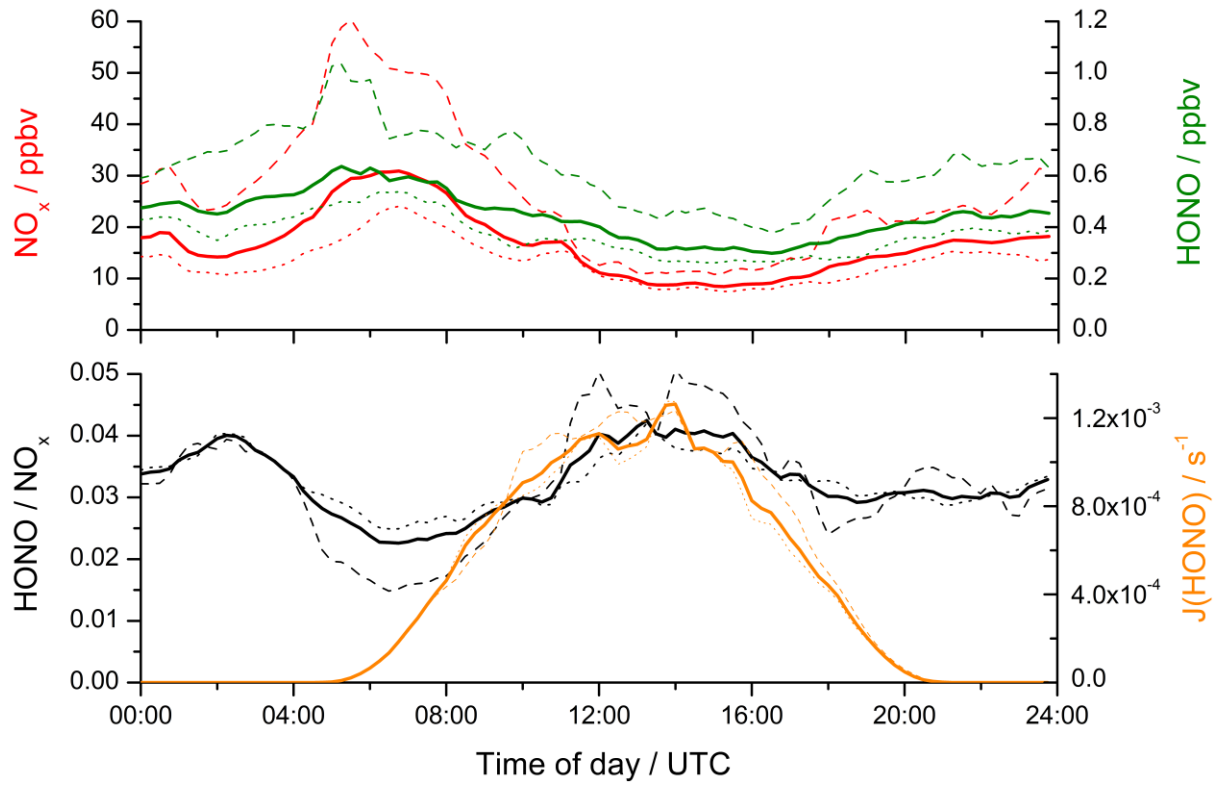
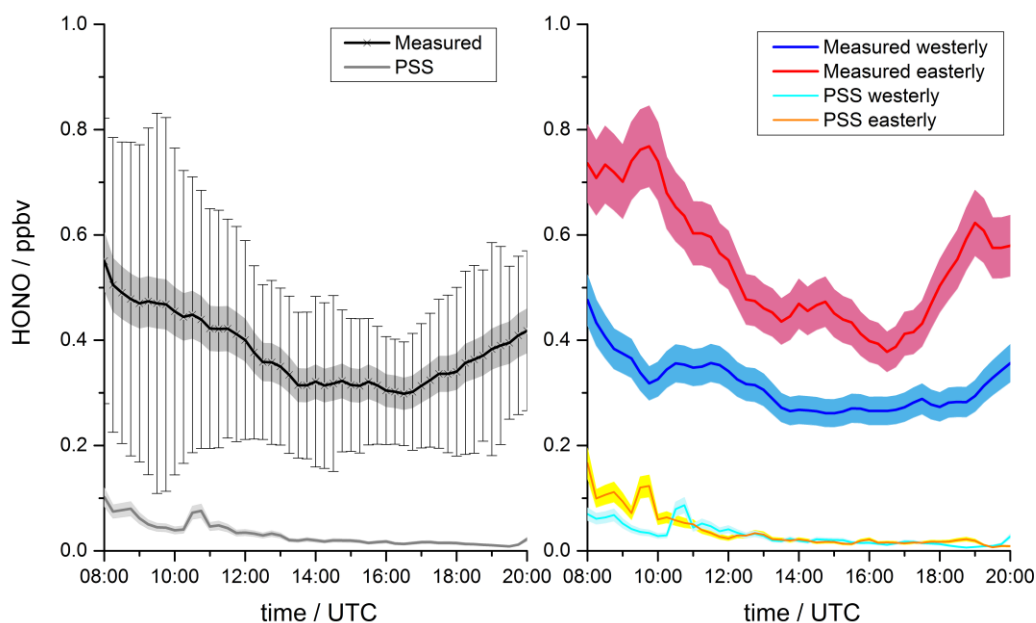


Figure 2. Average diurnal profiles of selected data from the IOP. The top panel shows total NO_x (red) and HONO (green) and the bottom panel shows $j(\text{HONO})$ (orange) and the HONO / NO_x ratio (black). Profiles were generated by binning all data in a 15 minute time period together. For each, the solid line is the total of all days, the dashed line is data from easterly conditions and the dotted line data from westerly conditions (see text for dates).

1



2

3 Figure 3. Averaged diurnal profiles (daylight hours) of measured (black) and photostationary
 4 state (PSS) calculated (grey) HONO (left panel). The shaded area represents instrumental
 5 ($\pm 10\%$) and model ($\pm 17\%$) error, the bars represent the standard deviation of the
 6 measurements. The right panel shows averaged diurnal profiles of measured and PSS HONO
 7 divided into easterly (red / orange) and westerly (blue / cyan) conditions. The shaded area
 8 represents the measurement ($\pm 10\%$) and PSS ($\pm 17\%$) error.

9

10

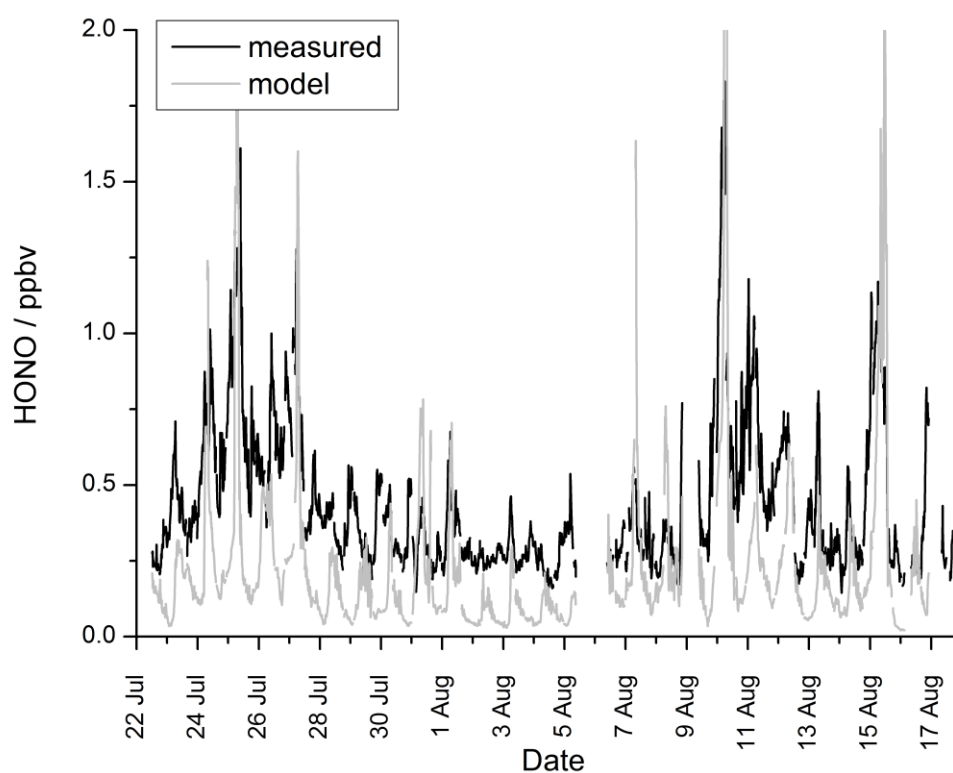
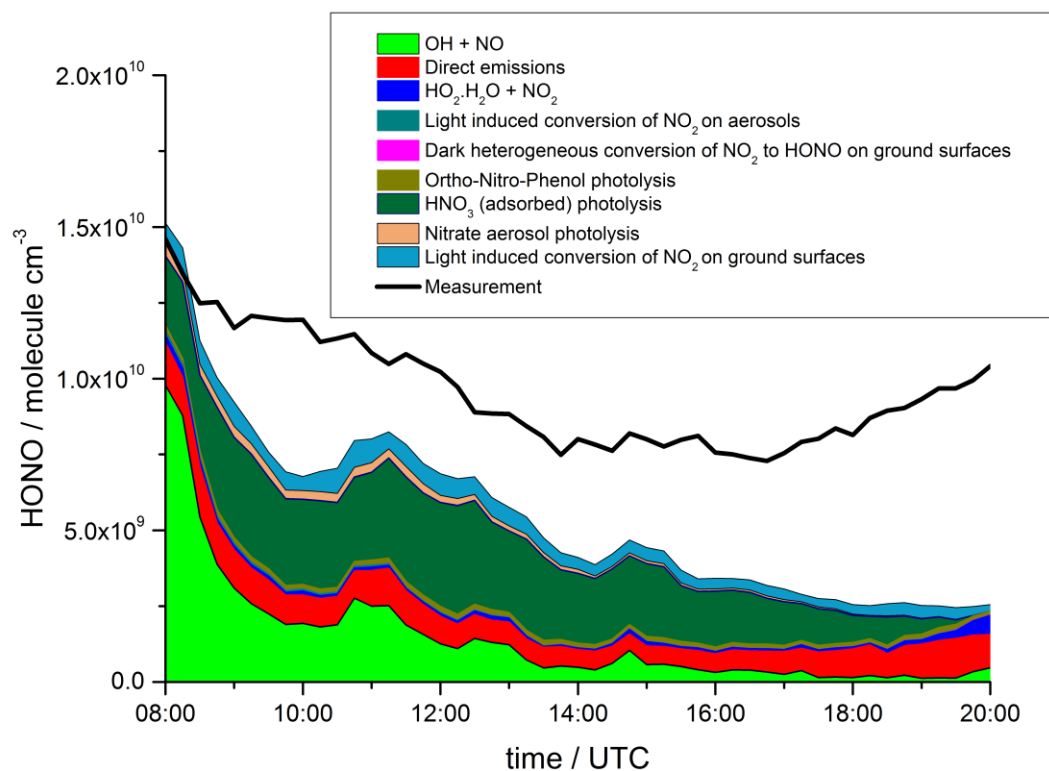


Figure 4. Time series of measured (black) and model calculated (grey) HONO during the IOP. The model was based on the Master Chemical Mechanism (MCM v3.2), see text for details.



1
2 Figure 5. Average daytime diurnal profile of the modelled HONO from different sources
3 shown as a compound area plot, as described in section 3.3 of the text. Also plotted (black
4 trace) is the measured HONO.
5

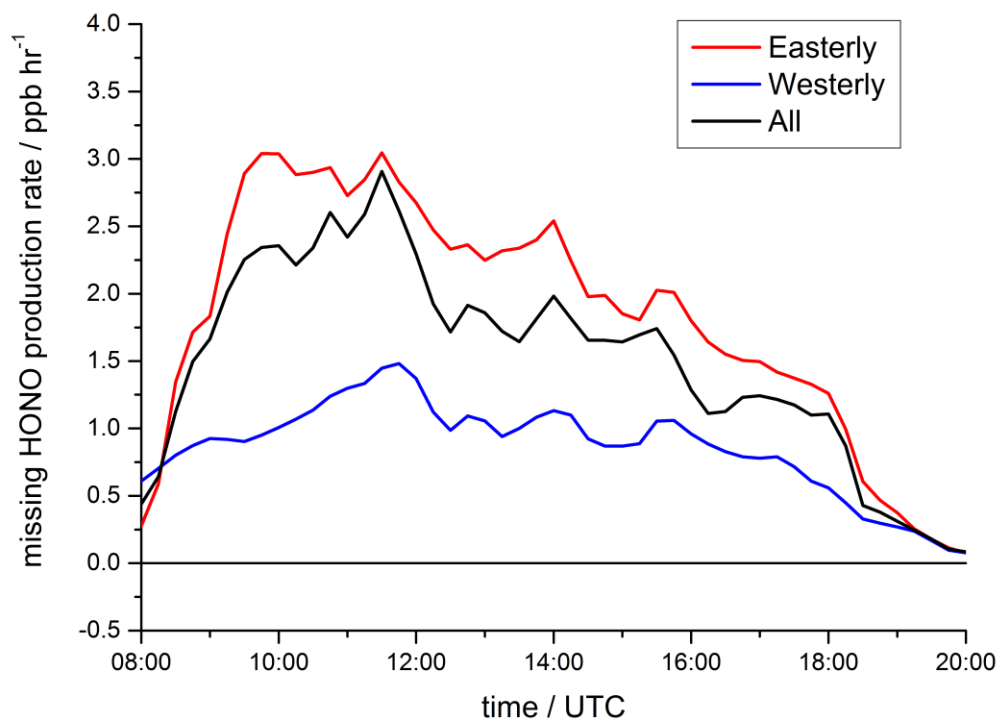
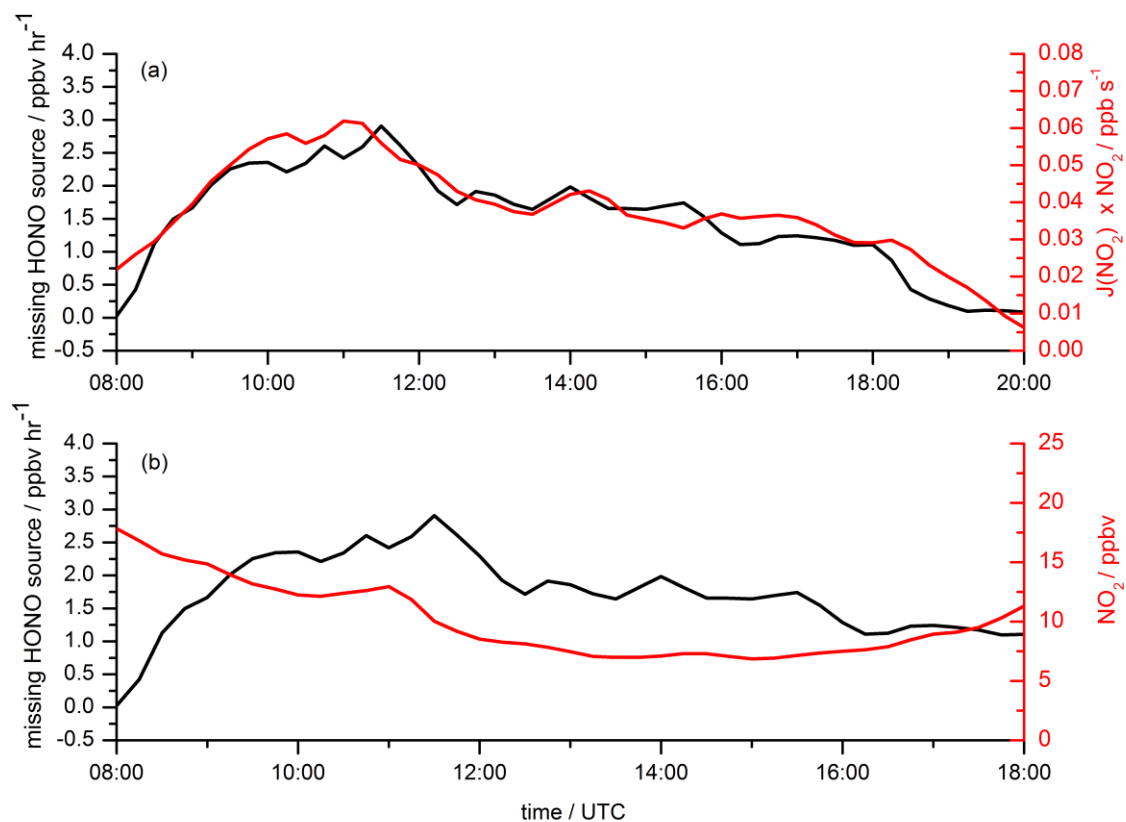
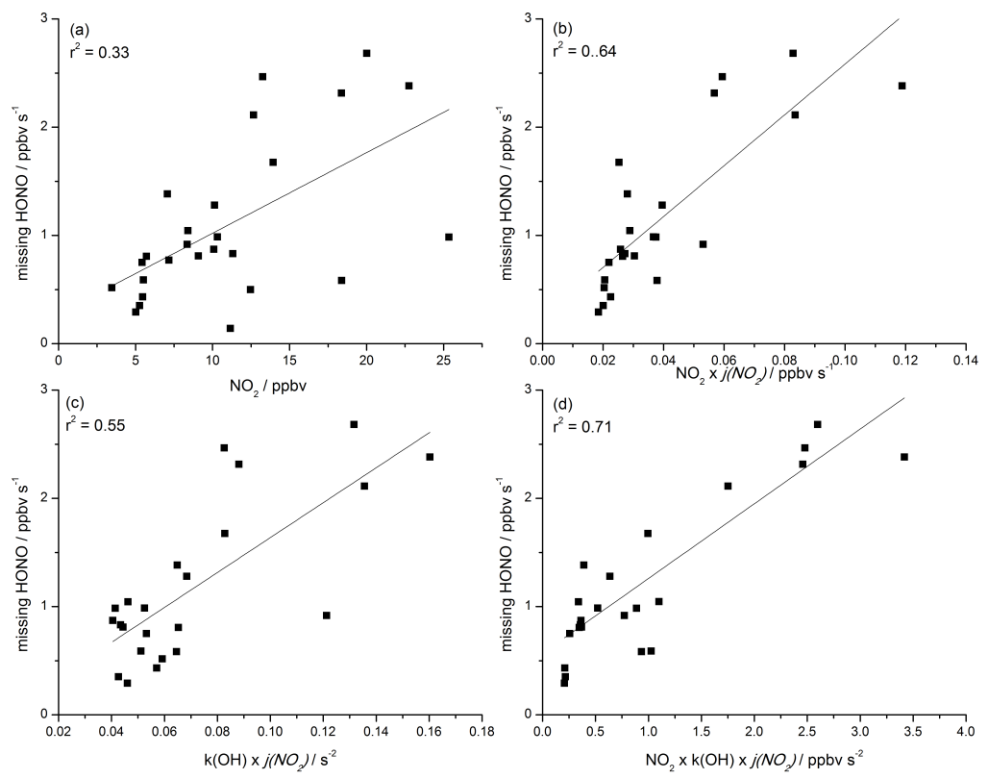


Figure 6. Average daytime diurnal profile of the ‘missing’ HONO production rate (in ppb hr⁻¹), defined as the rate of HONO production required to reproduce the measurements in the model. The black trace shows average of all data, the red trace shows the average of data from easterly conditions and the blue trace shows the average of data from westerly conditions.



1
2 Figure 7. Average diurnal profiles of the missing HONO source (black traces) plotted with (as
3 red traces) (a) $\text{NO}_2 \times j(\text{NO}_2)$ and (b) NO_2 .
4



1

2 Figure 8. Daytime averaged (08:00 – 19:00) missing HONO source plotted against (a) NO₂,
 3 (b) NO₂ × j(NO₂), (c) k(OH) × j(NO₂), (d) NO₂ × k(OH) × j(NO₂).

4

5

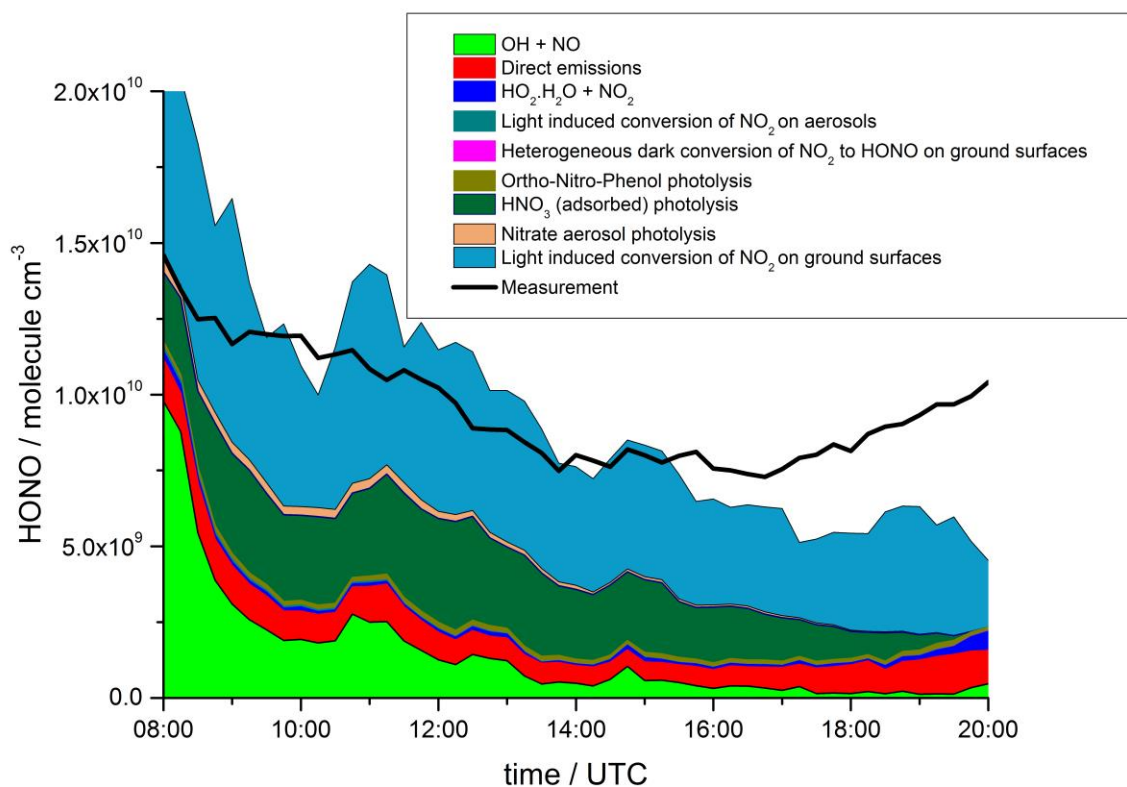
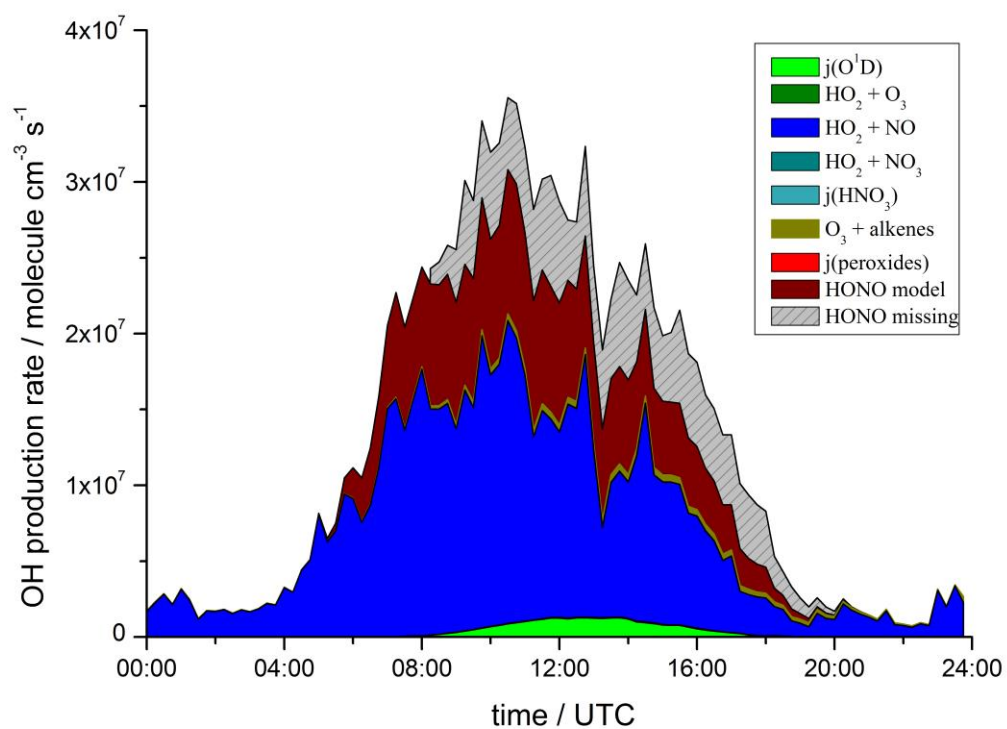
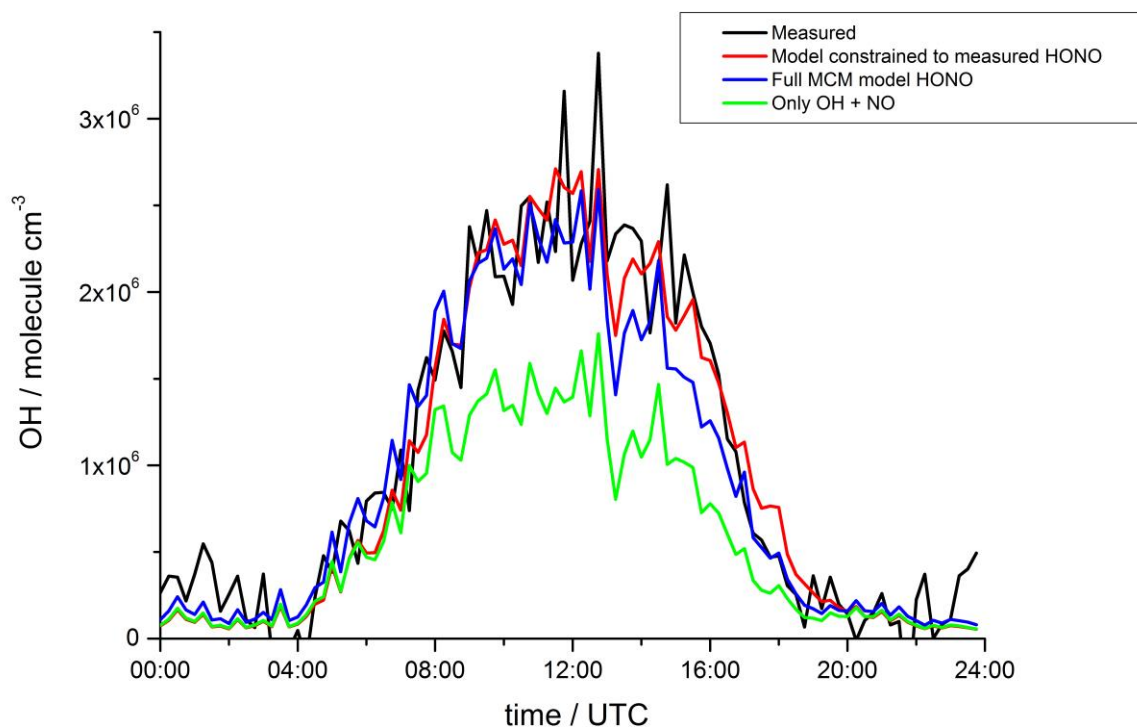


Figure 9. Average daytime diurnal profile of the modelled HONO from different sources shown as a compound area plot, as described in section 3.3 of the text, showing the result of increasing the reactive uptake coefficient of the light enhanced conversion of NO₂ on ground surfaces (see text for details). Also plotted (black trace) is the measured HONO.



2
3 Figure 10. Average diurnal profile of gross OH production rates from different initiation and
4 propagation sources calculated by the model.



2
3 Figure 11. Average diurnal profile of OH, showing measured (black), modelled unconstrained
4 to HONO with only NO + OH as a HONO sources (green), modelled unconstrained to
5 HONO including additional HONO sources (blue – see text for details) and model
6 constrained to measured HONO (red).